DEVELOPMENT OF A NOVEL BIAXIAL MECHANICAL TESTING SYSTEM AND PROTOCOLS FOR ANALYSIS OF BIOLOGIC TISSUES AND TISSUE-ENGINEERED CONSTRUCTS

A Dissertation

by

MINGLIANG JIANG

Submitted to the Office of Graduate and Professional Studies of
Texas A&M University
in partial fulfillment of the requirements for the degree of

DOCTOR OF PHILOSOPHY

Chair of Committee,	Michael R. Moreno
Committee Members,	Alan D. Freed
	Anastasia Muliana
	Alvin T. Yeh
	Ergun Akleman
Head of Department,	Andreas A. Polycarpou

August 2019

Major Subject: Mechanical Engineering

ABSTRACT

A new biaxial testing machine that is designed to experimentally investigate soft tissues is presented. The system is able to perform uniaxial, biaxial and simple shear tests as defined in a theoretical framework proposed by our collaborator. Proof-Of-Principle experiments have been carried out on silicone membrane. Testing protocols are also discussed in this research.

In addition, this research studies the various clamping methods for soft tissues. A novel clamp design for mechanical testing of soft biologic tissue that combines pins with serrated clamps to successfully decrease the occurrence of test sample slippage while reducing imposed stress concentrations at the clamping sites. The uniaxial tensile test is a standard method to obtain the mechanical properties of biological tissues and tissue-engineered constructs. Various clamping techniques have been developed in the past few decades to address the difficulty of imposing appropriate boundary conditions on soft tissues during mechanical testing. Two criteria for a successful clamping mechanism are (i) prevention of test specimen slippage, and (ii) prevention of test specimen failure outside the gage region. Informed by an extensive review of the related literature, this study presents a novel clamp design for mechanical testing of soft tissue. This design was validated by performing 40 uniaxial tensile tests on rat abdominal wall muscles using strain rates of 1% per second or 10% per second. Load and displacement data were acquired at the grips. The clamping area on the tissue sample was marked with India ink to track potential slippage of the sample during testing. Ultimate tensile strength and the corresponding stretch were calculated when the maximum load was achieved. With fine tuning of the torque applied to the clamping grips, the success rate of the tensile tests reached over 90%.

In this research, multiple strain measurement techniques for soft tissues are evaluated. Particularly, we investigated the strain measurement from both sides of soft biological tissue under uniaxial tensile test. Strain measurement is an important step in mechanical characterization of the mechanical behavior of soft tissues. Various strain measurement techniques have been developed in the past few decades. However, most of the research about strain measurement on soft

tissues are focused on only one side of the tissue (usually the side with less connective tissues). But what happened to the other side? After a brief review of the strain measurement on soft tissues, especially skins, this study presents measurement from both sides of rat skins under uniaxial loading environment. The motion of the four black markers glued on each side of soft tissues were tracked through optical approach. Finite element method was used to calculate the deformation of the quadrilateral formed by the markers. Twelve uniaxial tests were conducted and used for data analysis. Strain at both sides of the specimens were measured and compared. In general, when the stretch increased, the strain along the stretching direction (Exx) of both sides increased. However, the strain at the transverse direction (Eyy) and shear strain (Exy) behaved quite differently between the two sides. Thus, it might be necessary to take into consideration both sides when characterizing soft tissue mechanical properties.

DEDICATION

献给父亲姜家宝，母亲刘玲，以及外祖父刘志富。

ACKNOWLEDGMENTS

I would like to thank the entire Biomechanical Environments Laboratories research team, especially Dr. Michael Moreno, Dr. Steve Zambrano, Dr. Andrew Robbins, Caleb Davis, Hunter Storaci, Raghuveer Lalitha Sridah, Lise Ochej, Jordan Ankerson, Shannon Ingram, Zachary Lawson and Aaron Stone. Without all of you, this work would not have been possible.

I thank Dr. Moreno for his direction and support through my Ph.D. study. I would like to thank Dr. Freed for his suggestions and help on my research. I also would like to thank my committee members, Dr. Yeh, Dr. Akleman, Dr. Muliana for their help. And I would like to thank Dr. Benjamin for participating in my defense.

I would like to thank Mr. Erel Veysel (soon to be a doctor) for his help during my PhD study. I enjoyed the discussion with him about the research.

I appreciate my parents' continuous love, encouragement and support. This work could not be done without you. I feel very grateful to you.

CONTRIBUTORS AND FUNDING SOURCES

Contributors

This work was supported by a dissertation committee consisting of Professor Michael R. Moreno, Professor Anastasia Muliana, and Professor Alan D. Freed of the Department of Mechanical Engineering, Professor Alvin T. Yeh of Department of Biomedical Engineering and Professor Ergun Akleman of the Departments of Visualization & Computer Science and Visualization.

The rat abdominal wall tissues in Chapter 2 were collected from Tissue Sharing program in Texas A&M University.

All the work conducted for the dissertation was completed by the student independently.

Funding Sources

Graduate study was supported by a start-up funding from Texas A&M University.

NOMENCLATURE

DIC	Digital Image Correlation
VDA	Video Dimension Analyzer
TAMU	Texas A&M University

TABLE OF CONTENTS

Page

LIST OF FIGURES

FIGURE Page

LIST OF TABLES

TABLE Page

1. INTRODUCTION

1.1 Background

A report analysis indicates that the global tissue engineering and regenerative medicine market was worth $28 billion in 2018 and will grow to over $81 billion by 2023. In 2018, there are about 700 regenerative medicine companies around the world. Considering so much resource having been invested in this field, clinically efficacious tissue engineering solutions are conspicuously limited. To be clear, this investment has produced significant advancements in addressing the biochemical and immunologic concerns associated with tissue-engineered therapies. However, the ability to produce engineered constructs that mimic the complex mechanical behaviors observed in native tissues remains elusive. It is now evident that efforts to address challenges related to the mechanical performance of tissue-engineered therapies have been stifled by the relative absence of an appropriate mechanics framework from which to operate.

1.2 Innovations

The work proposed herein seeks to leverage the development of a new theoretical framework in non-linear mechanics that has been conceived to characterize the mechanical behaviors of biological tissues and tissue-engineered constructs. This framework employs physically meaningful parameters and provides unique insight for tissue engineering applications. In order to fully employ the concepts within this framework, novel mechanical testing systems and approaches are required. The importance of this work is the resulting systems and protocols will provide tissue engineers with important intuitive parameters to target in their design process that will enable unprecedented reproduction of the mechanical behaviors observed in native biologic tissues. The development of such systems and protocols is the primary goal of the proposed work.

1.3 Specific Aims

1.3.1 Develop a biaxial load frame capable of performing uniaxial, biaxial and shear tests on membranes, as defined in an appropriate theoretical framework

The theoretical framework employed to inform this work is unique in that complex deformations are described in terms of combinations of primary modes of deformation. In 2D, these modes are dilatation, squeeze and shear. This aim will be considered complete when a system is built that is capable of 1) testing the primary modes of deformation; and 2) performing the following loading profiles: strain rate sensitivity test, stress relaxation test, creep test, equi/general biaxial test, and shear test.

This aim was achieved without compromise. A biaxial mechanical testing system has been built. The system is able to perform the tests illustrated above.

1.3.2 Evaluate common sample clamping methods and identify an appropriate approach for soft tissue of interest

The ability to maintain a biologic tissue sample in a manner that is appropriate to obtain reliable data from mechanical tests represents a significant challenge. Different techniques have been employed by many groups with varying levels of success that are often unique to the specific application. This project is focused on the development of planar biaxial testing of soft tissues. Therefore this aim will be considered complete when multiple conventional clamping mechanisms are evaluated and an appropriate approach is identified for the tissue of interest. Such an approach may be a synthesis of the approaches evaluated or a novel approach optimized for the system developed in Aim 1.

This aim was achieved without compromise. A variety of clamping methods have been evaluated and a type of serrated clamps with needles is proposed for soft tissue clamping.

1.3.3 Evaluate the strain measurement techniques and identify an appropriate approach for soft tissue of interest

The ability to obtain the deformation of the soft tissues under complex loading environment still remains a challenge. There have been various strain measurement techniques such as optical marker tracking or digital image correlation developed and applied to biological tissues. This aim is considered complete when multiple strain measurement techniques are evaluated. the strain at both sides of the specimen could be different even under the same loading condition, especially, since biological tissues are multilayered, inhomogeneous and anisotropic, It is necessary to investigate the deformation of both surfaces.

This aim was achieved without compromise. A variety of strain measurement techniques have been evaluated. And experiments were performed to measure strain from both sides of multi-layered tissues.

1.3.4 Validate the system of Aim 1 using a conventional engineering material that has been well characterized

To the author's knowledge, there has not been any standard method for mechanical testing of biological tissues. Thus, it is still necessary to develop some test methods that can be used in our lab to consistently conduct mechanical testing. This aim is considered completed when 1) multiple testing protocols including uniaxial and biaxial testing have been designed; and 2) a conventional engineering material has been tested following these protocols:

1. 1D fiber protocols including viscoelasticity measures

   (a) Strain-rate sensitivity testing

   To investigate the effects of strain rate and history on our tissue constructs, samples will be stretched at the following strain rates: 1%, 3% and 10% per second.

   (b) Creep recovery testing

   Using the same system, specimens will be stretched uniaxially to a given load under load control.

(c) Stress-relaxation testing

Using the same system, specimens will be stretched uniaxially to a given load under load control.

2. 2D membrane protocols

(a) Equi-biaxial experiments (dilation only)

The sample will be stretched in two orthogonal directions by four linear actuators under centroid control. Force transducers will be set on each axis. The stretch ratio will be maintained such that there is a 1:1 correspondence between axes.

(b) General biaxial experiments (combination of squeeze and dilation)

Samples will be prepared and mounted to the biaxial load frame as described above. The membrane will be stretched in two axes with stretch ratios of 1:1, 1:0.5, 0.5:1 and 1:1, in total four test runs.

(c) Shear experiments

The specimen will be pulled from the center while fixed at the ends — a double-lap shear configuration.

This aim was achieved without compromise. Uniaxial and biaxial testing protocols have been developed.

2. DESIGN OF A BIAXIAL MECHANICAL TESTING SYSTEM

2.1 Introduction and Literature Review

2.1.1 Evolution of biological tissue mechanical testing

A variety of experiments has been performed to obtain the mechanical properties of biological tissues and tissue-engineered constructs in all relevant deformations[11, 12, 13, 14, 15, 16]. Uniaxial studies have been widely utilized to determine the mechanical properties of soft biological tissues and tissue-engineered constructs since it is convenient to control the boundary condition in one dimension[17, 18, 19]. This material testing method was founded from linear-elasticity theorems and was originally conceived to investigate the mechanical properties of isotropic, linearly-elastic materials under small deformations. However, biologic tissues are inhomogeneous, anisotropic, non-linear materials that typically undergo large deformations and are often subjected to complex multi-axial loading conditions. Thus, multi-axial testing methods are required to mimic the physiological-loading state in efforts to fully understand the mechanical behavior of the tissues and provide the information for development of constitutive laws and models.

In addition to multi-axial tensile or compressive loading, soft biological tissues and tissue-engineered constructs are also subjected to shear loading. Simple shear tests have been used to investigate the material response under shear loading[20, 21, 22].

2.1.2 Biaxial testing

It is not trivial to perform biaxial mechanical testing on soft biological tissues due to issues ranging from specimen preparation to establishment of operation parameters. Moreover, there is a lack of standard methodology for biaxial and shear testing on soft tissues.

2.1.2.1 Sample Geometry

The dumbbell shape is commonly used in standard uniaxial tensile testing[23]. In the center region of the specimen, the stress/strain is uniformly distributed. While, square and cruciform

shapes are most commonly employed and studied for biaxial mechanical testing.

Originally developed by Monch and Glaster[24], the cruciform shape has become widely used in biaxial mechanical testing of engineering materials. Based on the Saint-Venant's principle- “the difference between the effects of two different but statically equivalent loads becomes very small at sufficiently large distances from load”. As the arms are long, the stress distribution at the center region of the specimen may be assumed to be independent on the mode of applied load. The influence of gripping at the sample-grip contact sites could be neglected.

Avanzini and Battini compared samples in square (gripped by hooks), cruciform, cruciform-fillet, cruciform-tapered, and cruciform slits[25]. They observed that for the cruciform samples, those with tapered arm or slits behaved more extensively under the same load level, which is in accordance with their Finite Element Modeling. However, their simulation results show that cruciform-slits could improve the strain uniformity in the center region, while the cruciform-tapered sample result in a significant decay in strain and stress uniformity. Fillets on the specimen reduce stress and strain uniformity as well. Special care is necessary when mounting square specimens with hooks due to high sensitivity of the results to small deviation.

2.1.2.2 Boundary Conditions

The influence of boundary conditions of the soft tissue on mechanical measurement under biaxial loading has been experimentally studied and numerically investigated[26, 27, 28, 29, 30]. Soft-tissue related studies inherently involve small and slippery biological tissue samples; this makes it difficult to grip the tissue firmly and avoid stress concentrations. These difficulties lead to specimen damage, but more importantly, hinder the ability to obtain uniform boundary conditions. Suture-based methods and clamp-based methods have both been designed, utilized, and compared in the past[27, 28, 29].

2.1.2.3 Strain Field Homogeneity

Selection of the homogeneous deformation region within a specimen is also a source of difficulty. There are issues in the selection of the idealized center region as researchers are concerned

with stress and strain uniformity. Theoretically, the center region should be located far away from the edges of the sample. Finite element studies have been applied to explore the ideal area. Some researchers pick the 20% to 25% square region from the center[14, 31, 32, 33].

2.1.3 Simple shear testing

In previous simple shear tests, an in-plane moment is usually created when one clamp is fixed, and the other clamp was used to apply shear (add reference of Jimmy). In the current design, we propose a methodology to compensate for this moment based on Dokos *et al*'s experiments[34, 35].

As stated before, biaxial and simple shear tests have both been utilized to measure the mechanical properties of soft tissues. However, to the author's knowledge, they are usually performed separately, that is to say, there has not been any device which could incorporate both tests. In addition, the wide variety of testing methods applied in the past have largely not adopted a standardized procedure. The intent of this work is to: 1) design a system capable of developing idealized in-plane simple shear and 2) develop a testing protocol for the biomechanics community.

2.1.4 Current design's features

In the author's work, a biaxial mechanical testing device, as shown in Fig. 2.1, has been designed to be capable of performing a battery of experiments to characterize mechanical properties of biologic tissues under complex mechanical loading *in vitro*. In addition to the capabilities of a typical biaxial testing machine, the ability to perform simple shear has been added.

The following are the system design requirements:

1. Provide a versatile biaxial mechanical testing that incorporates uniaxial, biaxial, and simple shear test
2. Produce large displacement, i.e. 100 mm(3.94 in) for maximum displacement
3. Produce fast speed, i.e. 0.5 in/s for maximum speed
4. Provide a cost-efficient alternative to commercial biaxial mechanical testing devices
5. Propose a standardized testing methodology

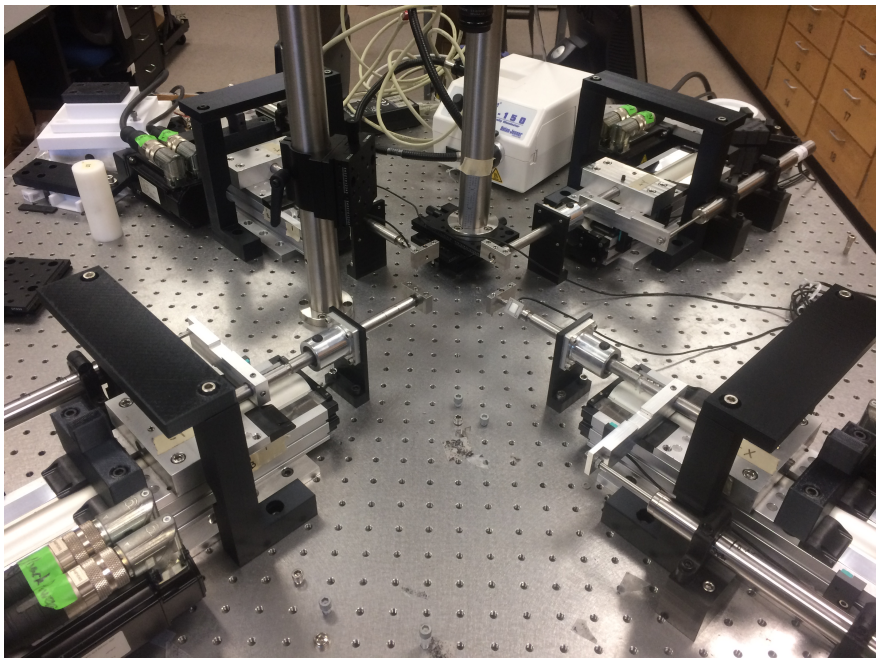

Figure 2.1: Biaxial testing system

The following will be discussed in this article: (a) system design; (b) experimental system capability; and (c) a case study of uniaxial, biaxial, and shear tests on silicone rubber.

2.2 Methods

2.2.1 System overview

System design allowed for non-contact measurement of mechanical properties from soft-tissue membranes in a two-dimensional plane and of most novelty, in-plane shear deformation. A system diagram is shown in Fig. 2.2. It consisted of four motorized linear actuators, each driven by a servo motor. The linear actuators were arranged around a center point on the breadboard with each stretching arm with one end connected to the carriage platform and the other reaching towards the center point. All linear actuators were rigidly affixed to a breadboard table to alleviate vibration. A camera was mounted above the specimen to record the markers'movement on the specimen. The system incorporated a custom four-axis controller that would enable load and displacement control on each axis. During the motion, the controller triggered the camera to synchronize the displacement and load measurement with imaging. The versatile system could be configured to

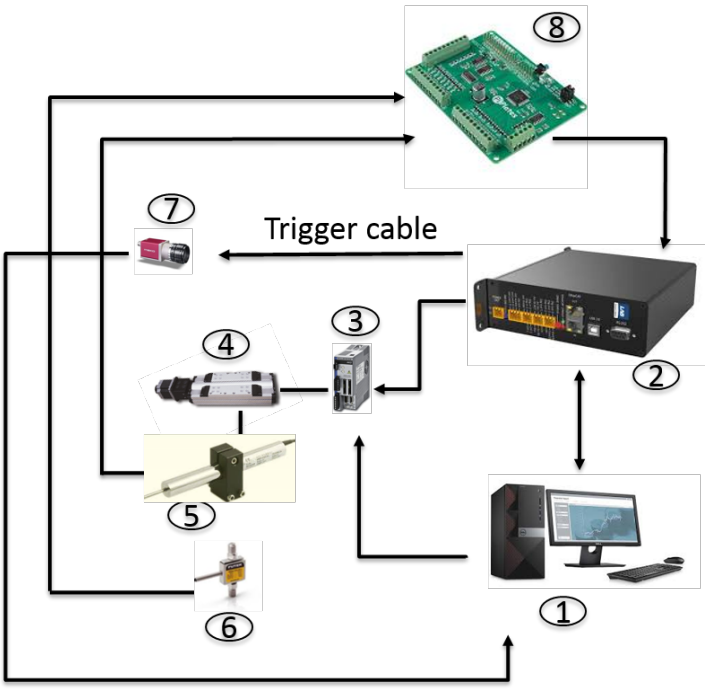

Figure 2.2: System diagram

conduct conventional uniaxial, equi-biaxial, general biaxial, and shear tests.

2.2.2 System hardware

2.2.2.1 Motion Components

This system was designed for precise load and displacement control for uniaxial and biaxial tests, with a capability for in-plane shear testing.

Four ball-screw linear actuators (DS4 series, Kollmorgen Corp., Radford, VA), each equipped with a 10mm lead and coupled with a servomotor (AKM23D, Kollmorgen Corp., Radford, VA), could achieve a maximum velocity of 0.5m/s, maximum carriage acceleration of 20 m/s^2, a resolution of 4um displacement and a range of 100mm. Each servomotor (AKM23D, Kollmorgen Corp., Radford, VA) was driven by a servo drive (AKD-P00306, Kollmorgen Corp., Radford, VA). Linear variable differential transformers (LVDT, MVL7C, Honeywell Sensing and Control, Columbus, Ohio), as shown in xx were employed for closed loop control of displacement. All the drives were controlled by a custom made four-axis digital servocontroller (MTI TESTExpress,

McGaw Technology Inc., Lakewood, Ohio).

2.2.2.2 Specimen Fixation

Custom, linear shafts operated as stretching arms; each were mounted onto the linear actuator carriage. Clamps were employed to connect the specimen to the stretching arm: each side of a specimen (cruciform) was gripped by a custom clamp which was attached to a linear shaft.

2.2.2.3 Strain and Displacement Measurement

Each linear actuator was connected to an LVDT, which was used to measure the stroke displacement and send signal feedback to the controller. An area scan camera (Basler acA1300-200um, Basler AG, Ahrensburg, Germany) fitted with a 25mm lens (HF25HA-1B, Computar, Cary, NC) was mounted above the specimen for non-contacting measurement.

2.2.2.4 Load Measurement

For biaxial mechanical testing, there was a uniaxial tension/compression load cell (Model 31, submersible, Honeywell Sensing and Control, Columbus, Ohio) on each orthogonal axis used to measure the force applied to the specimen. Uniaxial testing was accomplished in the same setup, but with only one set of linear actuators mirroring one another.

For shear testing, each side of a rectangular specimen was attached via clamps. A third clamp was attached to the central specimen region that allowed for force application perpendicular to the other axis established by the first clamp set. A uniaxial load cell is affixed onto this pulling axis to measure the force applied.

2.2.3 System software

2.2.3.1 Controller Software

The motion controller software (MTI TESTExpress Digital, McGaw Technology Inc., Lakewood, Ohio) had a stress-control function that sensed when load and displacement transducer output from opposing actuators were unbalanced. The detected signal difference was used in a closed-feedback loop to auto-correct actuator drives to a balanced state. The purpose of this con-

trol type was to protect the test system actuators from being subjected to bending forces by the opposing axis actuators. In addition, stress-control would keep the specimen gauge area stationary to allow for measurements via the system's camera.

The controller software was designed for use with a dedicated pair of parties (e.g., the Windows PC and the controller), and the two parties were connected by the Ethernet cable supplied with the controller, which was of the 'Crossover' type, intended for dedicated, two-party communication.

2.2.3.2 Strain Measurement

Tissue deformation studies do not generally employ strain gauges for strain measurement due to their mechanical interference with tissue deformation. Thus, a non-contact technique for strain measurement was chosen for this system. (A camera based experimental method for mechanical test on patellar tendons) Initially developed by Yin et al [9], the Video Dimensional Analyzer (VDA) technique was employed with a pair of video cameras independently monitoring and analyzing the distance between two parallell-painted lines on each axis to measure specimen dimensions in biaxial mechanical testing[32, 36]. Sacks developed a tracking algorithm by positioning a 50x50 pixel image sub-region on each marker and determining the location of the marker as the centroid of all the 0 intensity level pixels within its respective sub-region[33, 37, 38]. Humphrey et al developed a tracking algorithm to locate the center of the marker by searching through rows and columns and summing a row or column of pixel intensities. The pixel location corresponding to the maximum (light marker) or minimum (dark marker) sum is considered as the center.

However, the marker-based method has a drawback: due to the anisotropy and in-homogeneity, the local variation of soft tissue is difficult to completely examine. Thus full-field characterization was proposed to overcome this. Nielson et al developed a phase corrected cross-correlation technique to achieve a full-field strain measurement[39, 40]. Digital image correction (DIC) technique has also been applied to strain measurement of soft tissues[41, 42, 43].

In this article, a Digital Image Correction (DIC) software (Ncorr, Mechanical Engineering Department, Georgia Institute of Technology, Atlanta, GA) was applied to measure the strain.

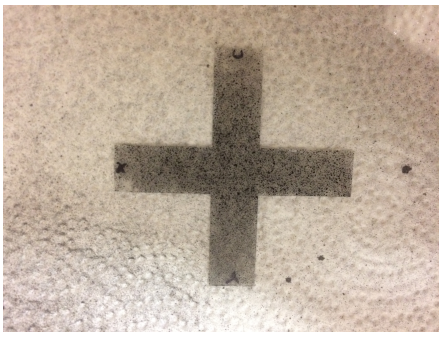

Figure 2.3: Cruciform specimen (painted with speckle pattern)

2.2.3.3 Feedback Control Modes

A PID controller was implemented to the system. As to uniaxial tests, the system provided both load and displacement control for each linear actuator independently.

As to biaxial tests, it also provided displacement control and stress control modes.

2.3 Specimen Preparation

Note in the following tests, all the specimens were laser cut from a silicone sheet with a thickness of 0.02" (Specialty Manufacturing Incorporation, Saginaw, MI). 1) rectangular specimens with dimension of 2 x 0.5" were used for uniaxial tests; 2) Cruciform specimens with arm with of 0.5", length of 2.5" and fillet of 0.01", as shown in Fig. 2.3, were used for biaxial tests; 3) rectangular specimens with dimension of 1.25 x 0.5" were used for simple shear tests. Three specimens were tested for each type of test. Specimens used for uniaxial strain rate sensitivity tests, biaxial tests and simple shear tests were painted with speckle patterns by spray paint.

2.4 Experimental System Capability

2.4.1 1D fiber protocols

2.4.1.1 Uniaxial Strain Rate Sensitivity Testing

To investigate the effects of strain rate and history on our tissue constructs, samples were stretched at multiple strain rates. Force and displacement data were acquired continuously throughout.

In this study, specimens were preconditioned to 70% strain (measured from grip distance) under 1%/s strain rate for ten cycles. Then specimens recovered for 15 min and then tested to 50% strain under 1%/s, 3%/s and 10%/s strain rates respectively with a recovery time of 15 min.

2.4.1.2 Creep Testing

Using the same system, specimens were stretched uniaxially to an identified stress level, and the stress was held constant for a period of time.

In this study, specimens were preconditioned to 40% strain (measured from grip distance) under 1%/s strain rate for ten cycles. Then specimens recovered for 15 min and then were raised to 40 psi in one second and held at this stress level for 30 min. Note the corresponding strain at 40 psi is about 25% strain, which fell into the preconditioned region.

2.4.1.3 Stress Relaxation Testing

Using the same test system, specimens were stretch uniaxially to an identified strain level, and the strain was held constant for a period of time.

Specimens were preconditioned to 40% strain (measured from grip distance) under 1%/s strain rate for ten cycles. Then specimens recovered for 15 min and then were raised to 30% strain in one second and held at the strain for 30 min.

2.4.2 2D membrane protocols

2.4.2.1 General Biaxial Experiments (Combination of Squeeze and Dilation)

Both displacement control and stress control were implemented in the tests. As to the displacement control, specimens were preconditioned to 70% strain under 1% strain rate for ten cycles and then recovered for 15 min. Then specimens were tested up to 50% strain under the following displacement protocol: $d_x : d_y$ = 1:1, 1:0.5, 0.5:1, and 1:1, where the subscripts x and y corresponds to the system's X and Y axes, respectively. Note the "1" refers to 50% strain level, and 0.5 refers half of the maximum strain, which is 25% strain. The recovery time between each test is 15 min. The testing protocol is shown in Fig. 2.4.

As to the stress control, the whole testing procedure consisted of the following stress control

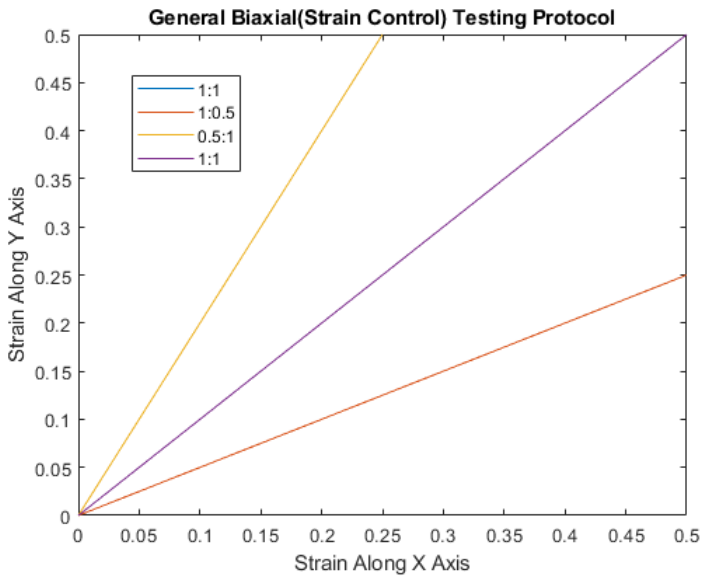

Figure 2.4: Strain-controlled general biaxial test protocols

protocols: T_x:T_y = 1:1, 1:0.5, 0.5:1, and 1:1, where the subscripts x and y corresponds to the system's X and Y axes, respectively. Note the "1" refers to 70 psi stress level, and 0.5 refers half of the maximum stress, which is 35 psi. Specimens were preconditioned for ten contiguous cycles for each protocol. The testing protocol is shown in Fig. 2.5.

2.4.3 Shear test

A custom fitting was attached to center of the specimen and mounted to a linear actuator. The specimen was be pulled from the center while fixed at the ends as shown in Fig. 2.6 — a double-lap shear configuration. Custom fixtures was designed to balance the pulling force such that the moment created from center loading will not damage the transducer.

Specimens were preconditioned to 15% strain forward and backward for ten cycles under 1%/s strain rate with triangular waves. Note here the strain is calculated as displacement of the center clamp (d_1) divided by the average of the clamp distance between the left and right clamps and the center clamp(d_2, d_3 respectively), as shown in Fig. 2.6. The specimens were rested for 15 min and tested to 15% under 1%/s strain rate. Special attention was paid to minimize the pre-stretch of the specimens at their sides, i.e., unmounted grip distance (the grip distance between the side

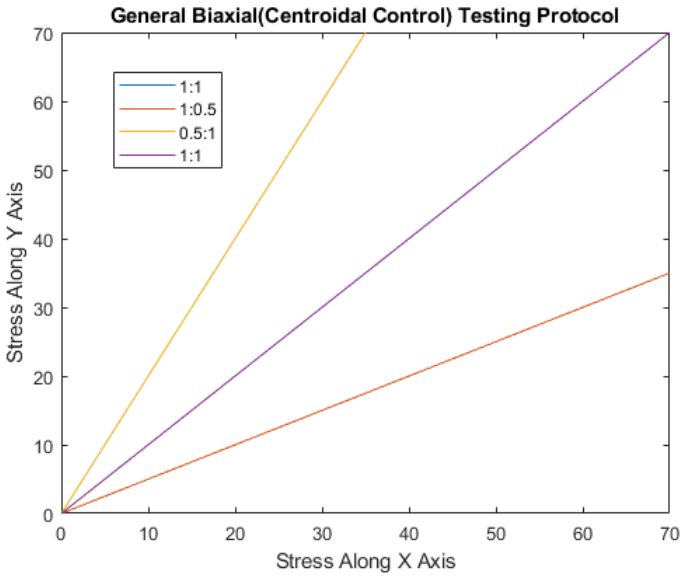

Figure 2.5: Stress-controlled general biaxial test protocols

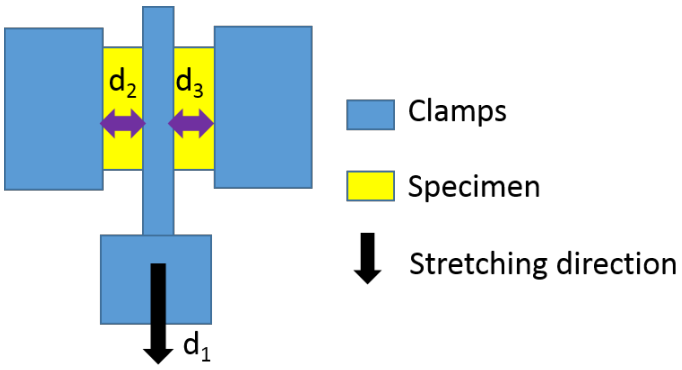

Figure 2.6: Double-lap shear configuration

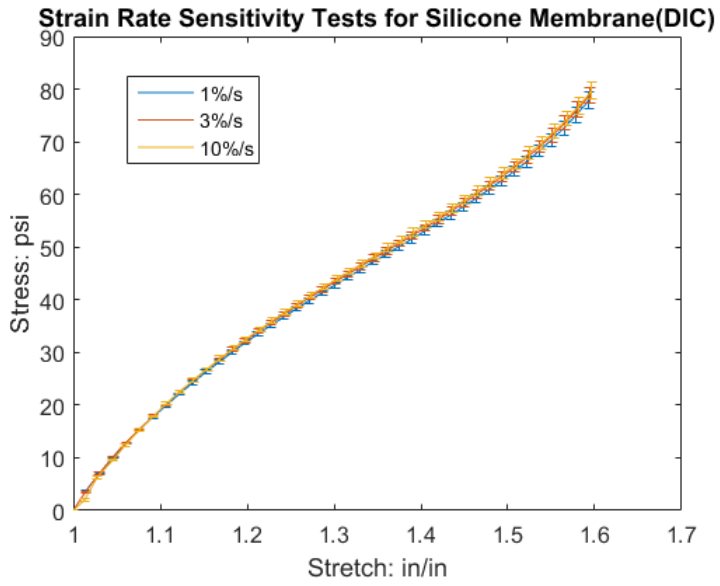

Figure 2.7: Uniaxial strain rate sensitivity test (strain measured from DIC)

clamps before the specimen was mounted to the experimental setup) and mounted grip distance were compared to ensure the pre-stretch was within a small range, less than 1%.

2.5 Results and Discussion

2.5.1 1D tests

2.5.1.1 Uniaxial Strain Rate Sensitivity Tests

The uniaxial strain rate sensitivity tests are shown in Fig. 2.7 Note in this figure, the strain data was obtained for digital image correlation(DIC) analysis on a selected region of interest(ROI)(Fig. 2.8). The figure shows no significant difference between specimens at the three strain rates. Thus the silicone membrane we tested was not very sensitive to strain rates within this range of strain rates.

We also plotted the stress-strain curves of these specimens using grip distance(Fig. 2.9). By comparing the stress-strain curves between these two figures, we concluded that for rectangular specimens used in this test, the strain measured from grip distance was very close to that measured by digital image correlation within this test range. Thus we could simplify the strain of rectangular

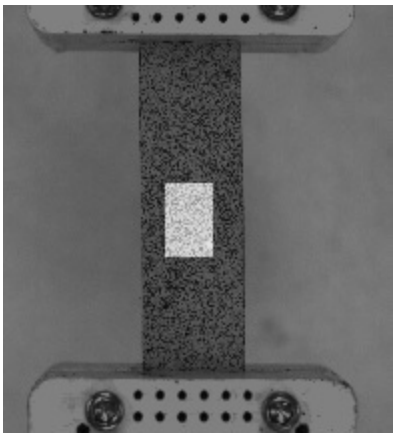

Figure 2.8: Selected region of interest of uniaxial tensile test

specimens by using grip displacement within this test range.

2.5.1.2 Stress Relaxation Tests

The stress relaxation tests are shown in Fig. 2.10. The stress here was calculated as measured load divided by the original cross section area. The figure shows that the stress had a sudden rise in the beginning and then decreased slowly to 46.5 psi after 30 min.

2.5.1.3 Creep Tests

The creep tests are shown in Fig. 2.11. The stretch here was calculated as grip displacement divided by the original grip distance. The figure shows that the strain had a sudden rise in the beginning and then increased slowly to 0.253 after 30 min.

2.5.2 General biaxial tests

The strain-controlled general biaxial(including equi-biaxial) tests are shown in Fig. 2.12 and Fig. 2.13. Note in Run1(equibiaxial tests), the stress-strain curves between X and Y axes are very similar. In Run2, when Axis X was subjected to 50% strain, and Axis Y was subjected to 25% strain, the center region of the specimens in X axis was stretch to 1.275 while in Y axis was stretched to 1.025. Vice versa, in Run3.

The stretch ratio was obtained from DIC analysis on a selected ROI(Fig. 2.14. The stress was

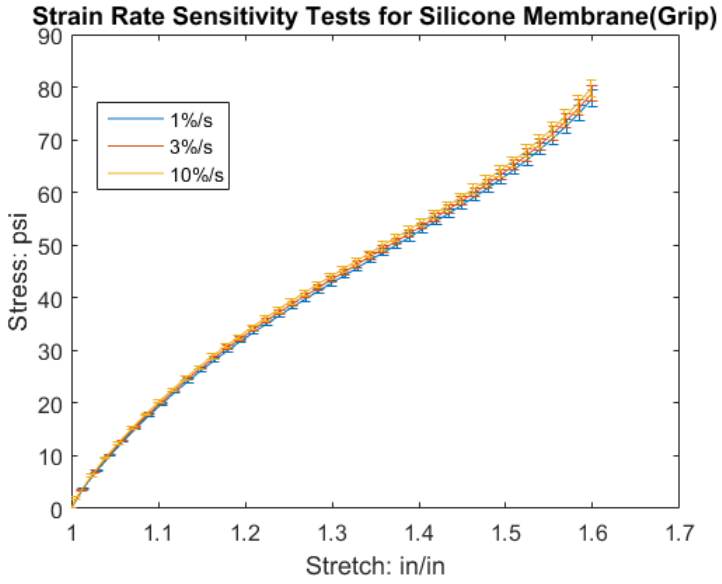

Figure 2.9: Uniaxial strain rate sensitivity test (strain measured from grip distance)

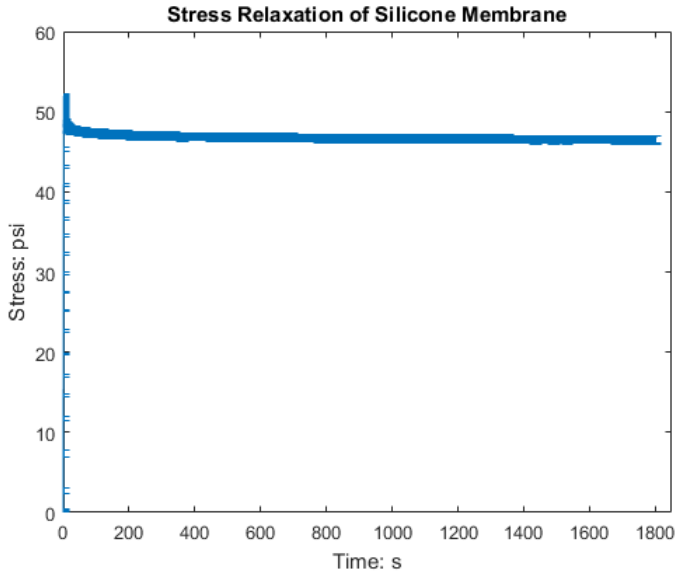

Figure 2.10: Stress relaxation tests of silicone membrane

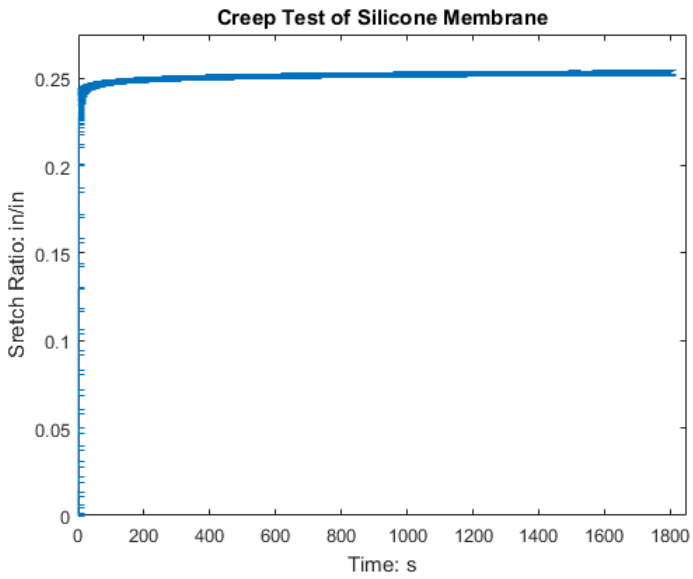

Figure 2.11: Creep tests of silicone membrane

calculated as load measured at the grips divided by the cross-section area of the arms of a crucifrom specimen. Between Run1 and Run4(equibiaxial), the stress-strain curves almost overlapped.

The stress-controlled general biaxial(including equi-biaxial) tests are shown in Fig. 2.15 and Fig. 2.16.

Note in Run1(equibiaxial tests), the stress-strain curves between X and Y axes are very similar. In Run2, when Axis X was subjected to 70 psi, and Axis Y was subjected to 35 psi, the center region of the specimens in X axis was stretched outwards while in Y axis was stretched inward. Vice versa, in Run3. Between Run1 and Run4(equibiaxial), the stress strain curves shifted towards right. As the specimens were under cyclic loading, they became softer. Thus under the same stress level, they would be stretched more in the later cycles.

2.5.3 Simple shear tests

The stress-strain curve for simple shear test is shown in Fig. 2.17. The curve in general shows a linear relation between the shear stress and shear stretch under a small strain. The shear strain was obtained from DIC analysis on a selected ROI(Fig. 2.18). The shear stress was calculated as the load measured at the central grip divided by the cross section area of the gripped specimen and

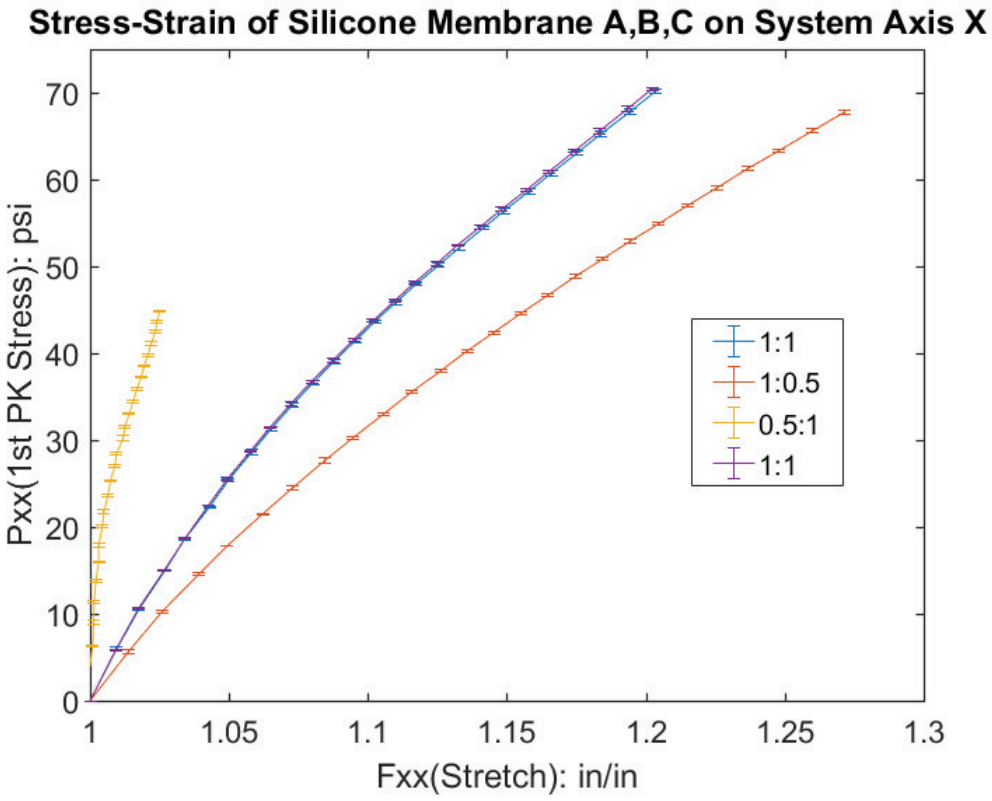

Figure 2.12: Strain-controlled general biaxial test - X axis

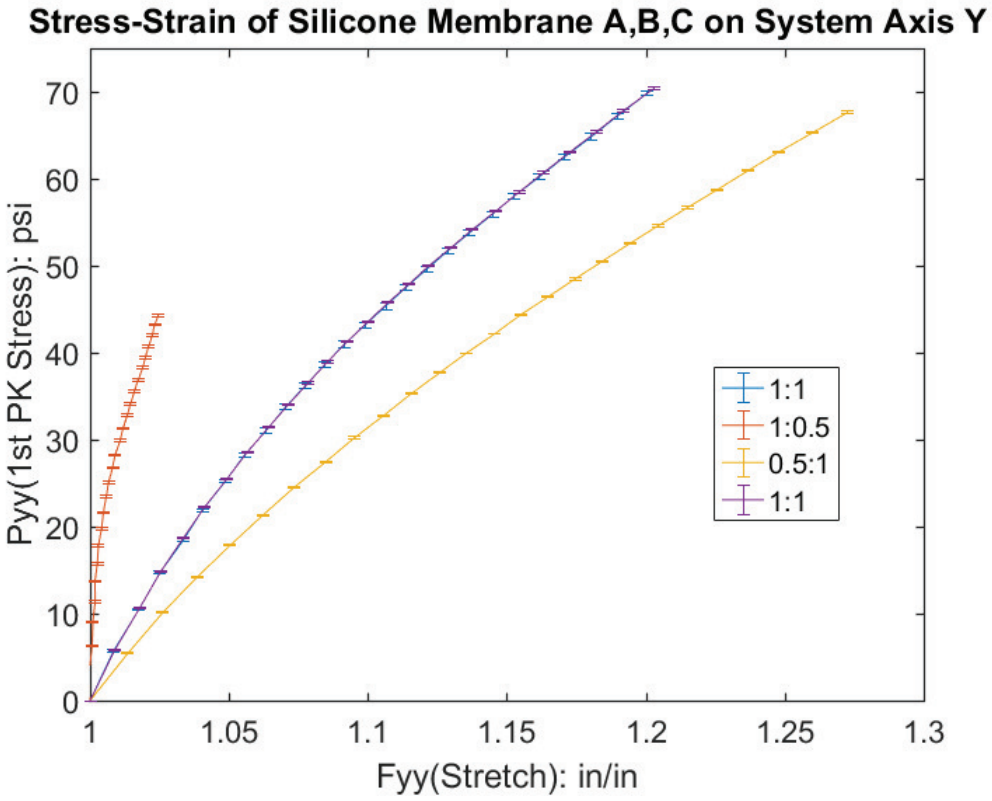

Figure 2.13: Strain-controlled general biaxial test - Y axis

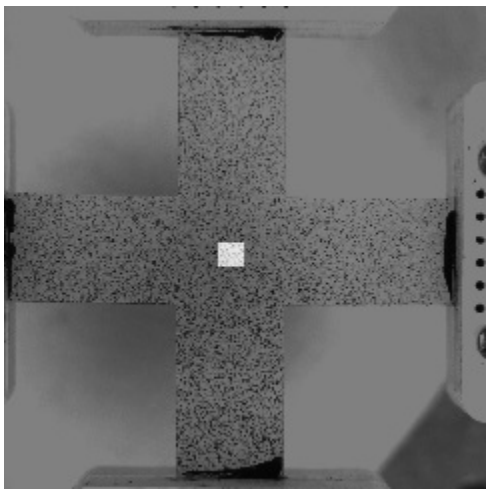

Figure 2.14: Selected region of interest for biaxial test

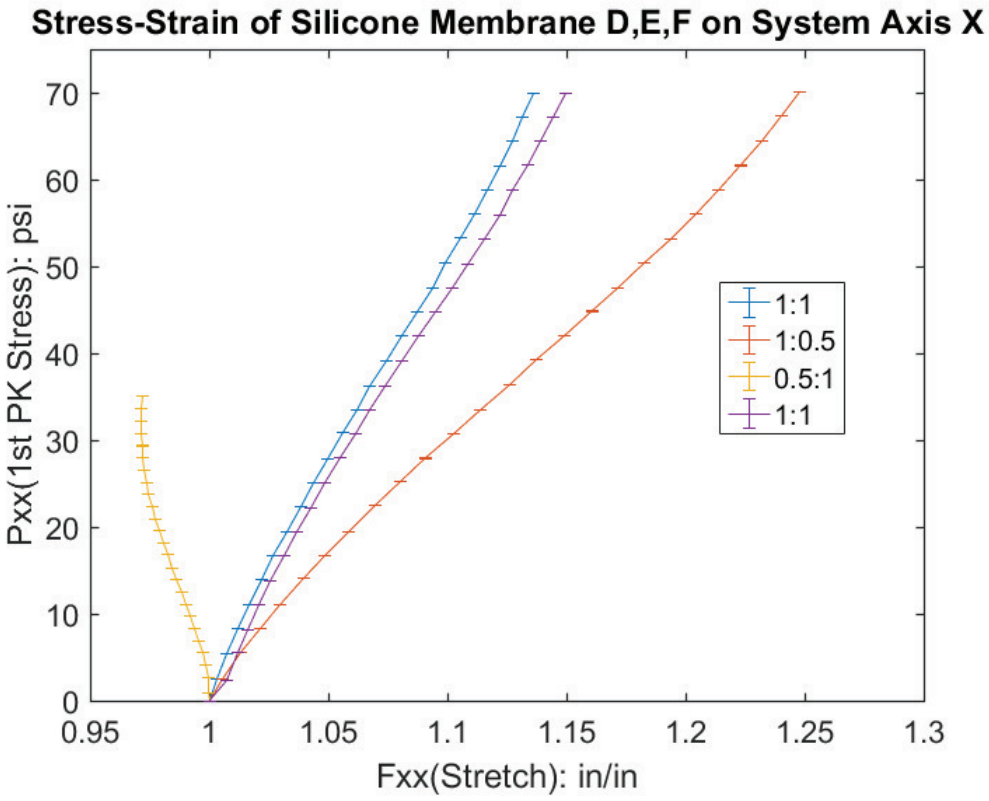

Figure 2.15: Stress-controlled general biaxial test - X axis

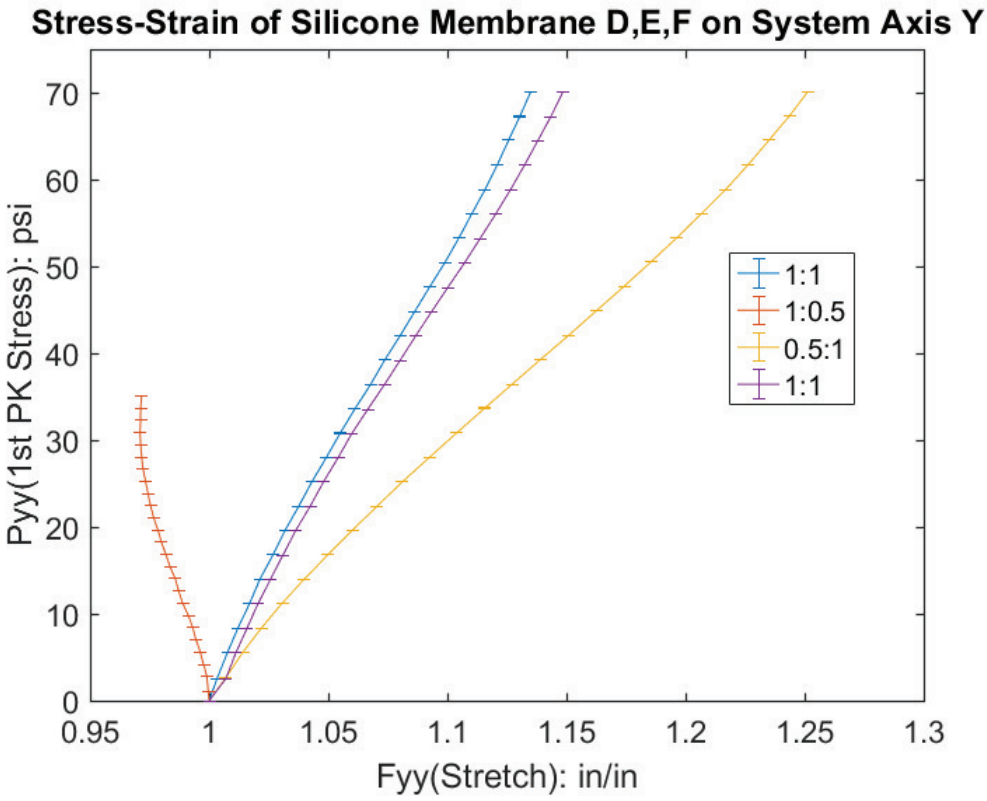

Figure 2.16: Stress-controlled general biaxial test - Y axis

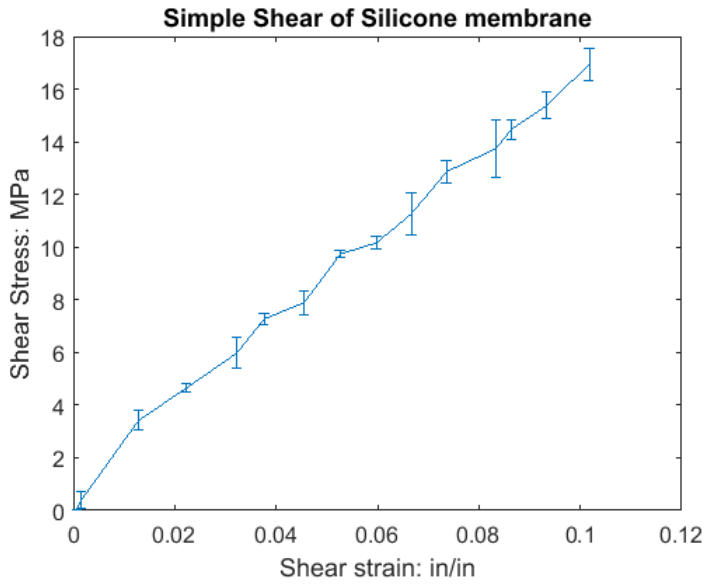

Figure 2.17: Stress-strain of simple shear tests

divided by two. Note the shear in the region of interest is smaller than the shear applied through grip displacement.

2.6 Conclusion

An experimental apparatus was designed with the intention of performing both biaxial and simple shear tests. A number of mechanical considerations were taken into account in the design of this setup. Proof-Of-Principle tests have been conducted to evaluate this system.

This work represents a significant step in mechanical testing of engineering materials and soft biological tissues. The results from future work with this system will lead to a better understanding of the mechanical properties of soft tissues under complex loading environments.

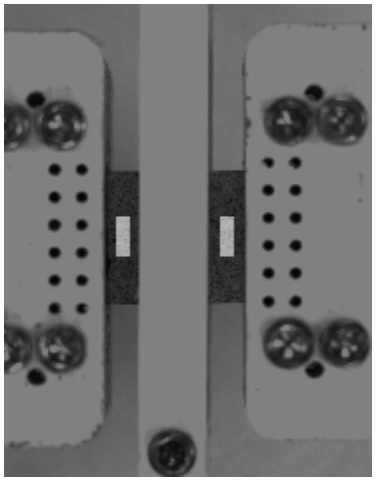

Figure 2.18: Selected region of interest of simple shear test

3. FIXING SOFT BIOLOGICAL TISSUE FOR MECHANICAL TESTING: A REVIEW OF CURRENT METHODS AND DEVELOPMENT OF A NOVEL CLAMPING MECHANISM

3.1 Introduction

Clamping has been widely employed in uniaxial tensile tests of a variety of soft tissues and tissue-engineered constructs. The clamping approach is generally chosen to ensure a continuous and uniform lateral load distribution at the junction of the clamp and the sample by constraining the clamped edges of the sample[44]; however, soft tissues often pose unique challenges. The central difficulty arises from the low friction between the surface of the clamping device and the soft biologic tissue specimen, leading to slippage of the sample during testing. A common solution is to increase the clamping pressure; however, this may induce significant deformation or a serious distortion of the clamped portion of the sample, resulting in premature failure. The specimen may be flattened and extruded beyond the edges of the clamps to the extent that water is squeezed from the tissue. The resulting reduction in cross sectional area at the clamped ends may convolute the mechanical characterization of the specimen[45]. Such problems compound for thicker specimens, as the load is distributed unevenly over different layers of fibers. When clamped tightly, no obvious slippage is observed at the superficial fibers; however, due to the high compression at the surface, the shear between the external sample contact surface and the internal sample core might result in slippage of inner fibers. In such cases the results obtained would not reflect the true mechanical behavior of the tissue as a whole [7]. In summary, a successful uniaxial tensile test occurs when both (i) the specimen fails in the gage region and (ii) no slippage is observed. Merely increasing clamp pressure might not be sufficient to guarantee a successful test. In response, researchers have developed a variety of alternatives for addressing the potential problems related to sample fixation when conducting mechanical tests of soft tissues.[2, 8, 46, 3, 47].

3.1.1 A brief review of conventional clamping methods

Generally, techniques used to fix soft tissues for mechanical testing can be grouped into the following classifications: (i) modifying the clamp interface geometry, (ii) adding additional materials such as sandpaper or adhesive, and (iii) altering the specimen's mechanical properties in the clamped region to be more conducive to mechanical fixation. Importantly, these techniques are not mutually exclusive and are often employed in tandem. The first classification includes methods such as screw-tightened [2, 3] or self-tightened clamps [48, 6, 4] with flat or serrated teeth (in sinusoidal or trapezoidal shape) [2, 3, 1]. The second classification includes methods such as adding sandpaper [49, 50, 51] between the specimen and the clamp, gluing the sample [52, 45] and coil binding the sample. [53, 54, 53]. The third classification includes methods such as such as air-drying to prepare the ends of the specimen prior to securing it [55, 56], employing cryogenic fixation devices as a means of freezing the clamped ends of specimen [7, 57, 58, 59], and use of low cost thermoelectric clamps. [8, 55].

3.1.2 Increasing surface friction or adhesion

3.1.2.1 Serrated Clamps

Serrated clamps have been used to increase both the contact area and friction between the specimen and clamps. Researchers proposed serrations in triangular [60], sinusoidal[1] or trapezoidal shapes [2]. Butler *et al*[1] designed grip insert teeth in a sinusoidal shape with smooth surfaces and pinned them into modified Instron wedge action jaws. The peaks of the insert teeth were rounded off and a larger radius of curvature was created at the exit tooth to reduce the stress concentrations. An example of Butler *et al*'s design is shown in Fig. 3.1. [61, 2].

Metal serrated clamps have been commonly used[62, 60], though plastic serrated clamps were proposed as a means to avoid cutting into the specimen in the early 1970s by Blanton and Biggs[61]. Cheung and Zhang[2] used a non-frozen, plastic serrated jaw clamp which had the advantage of simple fabrication and adjustment, as shown in Fig. 3.2. They achieved over 2.5kN and about 30% strain without observed slippage. Instead of making serrations of metal clamping plates post-

Figure 3.1: Butler's metal serrated clamps, reprinted with permission from [1]

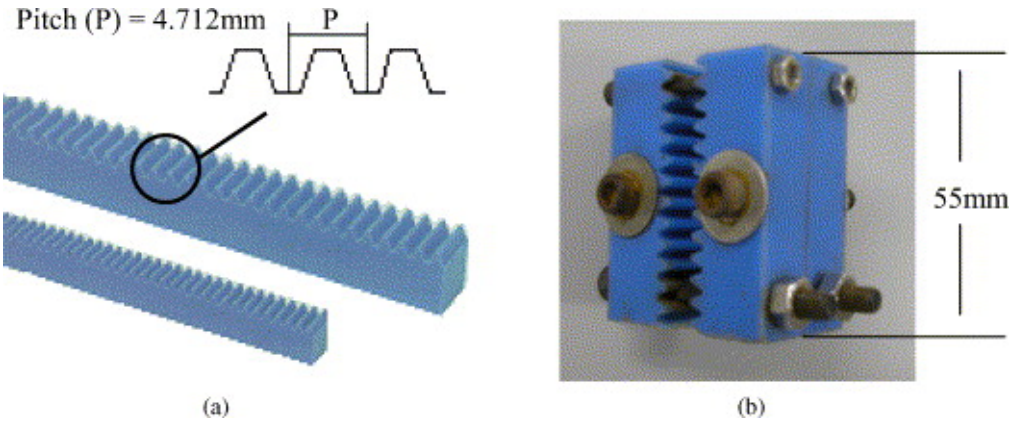

Figure 3.2: Cheung's plastic serrated clamps, reprinted with permission from [2]

machining, which is common in literatures, they used pre-molded gear type serrations and plastic material since which can provide completely closed peak-valley position and reduce the stress concentration effect at the clamping sites, thereby avoiding cutting of the specimen.

While peak-to-valley style[2] has been commonly used, Shi *et al* proposed a peak-to-peak style [3] in 2012, as shown in Fig. 3.3 They reported that the tissue at the peak-to-peak part of the clamp tended to be less wet, harder and thinner than the valley-to-valley portion, which increased the friction. The valley-to-valley part of the tissue became thicker and constrained in limited space due to the displacement of the water; this effect maintained high pressure within the airtight valley-to-

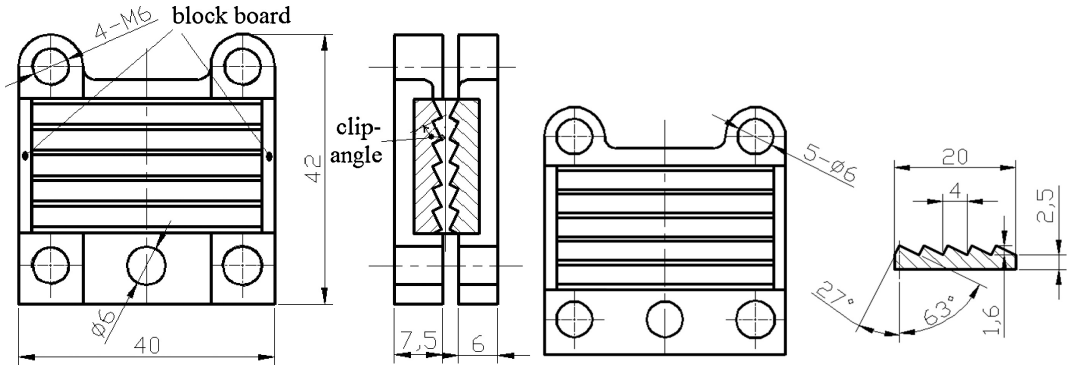

Figure 3.3: Shi's peak-to-peak clamps, reprinted with permission from [3]

valley space, which also helped prevent slippage. The design change proved beneficial as it could sustain a targeted tensile force of at least 4.0 kN without slippage, compared to 2.5 kN for the peak-to-valley design proposed by Cheung and Zhang[2]. Selected serrated clamps are presented in Table 3.1.

Table 3.1: Selected clamping methods

Clamping technique	Citation	Device description	Specimen type	Results
Serrated Clamps	Ker 1986	A serrated steel plate and a flat dural plate, a rectangular aperture at the front edge of clamps	Leg tendons of male wallabies	The shape of aperture has to be reasonably matched the specimen shape
	Butler 1984	Grip teeth in sinusoidal shape with smooth surfaces	17 gracilis tendon, 11 semitendinosus tendon, 14 patellar-tendon bone, 18 fascia lata	Slippage: 3 gracilis, 7 semitendinosus and 11 fascial. None in patellar tendon-bone tendon
	Cheung 2006	Plastic jaws with pre-molded gear type serrations	Bovine tendon	In test I, the grip achieved strain of about 30% without slippage. In test II, it achieved about 20% strain before slippage
	Shi 2012	peak-to-peak jaw clamp	Five cattle tendons	No visual slippage happened before a load of 4.0kN
Sandpaper Technique	Viidik 1967	multilayer textiles and paper with hard aluminum clamps	Hind limb tendons of rabbits	45 of 101 (45%) specimen failed in free space
	Iatridis 2003	Grips covered by neoprene rubber	Subcutaneous connective tissue from the abdomen of five male rats	No slippage
	Lyon 2014	Grips covered in grade P60 sandpaper	Porcine rectus sheath	Some cases of slippage (not specified)
Adhesive Techniqe	Soden 1974	Coating the ends of the specimen with Eastman's 910 adhesive and clamping them to plastic end plates with small metal damps	Various connective tissues such as fascia, tendon, sclera and so on	Failures rarely occurred at the grips
	Scalise 2015	Embedding tendon ends in a synthetic resin inside custom designed clamps	Ten patellar tendons were extracted from five healthy rabbits, 3–4 months old (3.5 - 0.5 kg)	One sample slipped
Winding Technique	Benedict 1968	Each end of the tendon was wound tightly, in coil fashion, with number 36 copper wire, for a distance of about 1/2 in. from the end	The M. extensor digitorum longus M. extensor digitorum brevis, M. extensor hallucis longus, M. Bexor digitorum longus (common), and M. flexor hallucis longus	Failure at the jaws in very few tests, slippage in certain tests
	Cohen 1976	The first 4mm of both free ends were wound with 0.009 in dia. nylon monofilament	Human flexor digitorum sublimus tendon from hands of a male of 21yr, a male of 55yr, a female of 89yr, bovine deep flexor foot tendon from a mature animal and a tape of purified steer tendon (prepared by Ethicon.Inc., Somerville. NJ)	No slippage of the specimen within the clamp

Table 3.1 Continued

Clamping technique	Citation	Device description	Specimen type	Results
Self-Tightening Clamps	Wright DG 1964	Two wedge-like teeth jaws were set inside the recess of a block	Plantar fascia	All failures occurred at the edge of clamps, cannot be considered as true failures
	Abrahams M 1967	Spring-loaded wedge-shaped jaws	Horse tendon and human tendon	The function of these grips in preventing slippage and damage was limited as they noticed that when the strain level went beyond 4.0-5.0%, the clamped part of the specimen was damaged and slippage occurred in some cases
	Woo 1980	Pivot clamps	One year old Yucatan swine tendon	All failed successfully
	Svendsen 1984	Steel clamps, an inner part with a conic projection and an outer part with a recess	Upper third of Wistar female rat tails	No slippage, final rupture occurred between the clamps
	Schechtman 1994	Pairs of wedges with sand-blasted, rigid, flat gripping surfaces and a housing	Human extensor digitorum longus and extensor halluces longus tendons	All specimens ruptured in the free-length region. No slippage
Dehydration Technique	Wang 1995	The portion of tendon under each clamp was first air-dried and wrapped with masking tape, while the midsection was kept moistened with saline	Six wallaby tail tendons	Most of the tendon broke in the central third of the length between the clamps. (>90%)
	Ker 2000	Air dry the ends to be clamped, whilst the rest of the specimen is kept moist by being wrapped in a damp tissue. Each dried end was clamped between flat steel plates with shallow transverse serrations screwed firmly together	Wallaby hind limb tendons and tail tendons	Not specified
Freezing Technique	Riemersa 1982	Indented brass plates, one of them with a cavity to hold liquid CO2	Horses digital flexor tendons	A tremendous tensile force of 13,800N was achieved without slippage
	Wieloch 2004	Two copper plates, a container for liquid nitrogen was soldered to outside of each plate	The Achilles tendons of 88 male Sprague–Dawley rats	In 176 testing, no slipping was registered

Table 3.1 Continued

Clamping technique	Citation	Device description	Specimen type	Results
	Sharkey 1995	Clamps fabricated from Aluminum, cooled with liquid nitrogen	8 shoulders, 7 elbows, 8 knees and 11 feet from eight fresh cadaver	95% success rate. Forces exceeding 3,500N were applied to knee, and forces exceeding 2,000N were applied to Achilles without failure or apparent slippage
	Staubli 1996	The specimen was set in aluminum blocks which were cooled by liquid nitrogen to -196°C, Then water was poured to form an ice block immediately, which secured the end of the specimen	16 unconditioned and preconditioned 10-mm-wide central sections of quadriceps tendon-bone (QT-B) and bone-patellar ligament (B-PL) complexes from young male donors (mean age 24.9 years, range 19-32 years)	26 of 32 failed at midsubstance. No slippage
	Ramachandran 2005	It consists of a top and bottom cryofixation assembly. Each assembly consists of two main segments: a nitrogen container which is used to circulate coolant, liquid nitrogen and an ice container where the specimen is fixed	10 rabbit Achilles tendon	All midsubstance failure, no slippage
	Kiss 2009	Modified a TEC VGA waterblock (MCW50-T, Swiftech, Lakewood, CA) into a device which was composed of a custom-made aluminum serrated plate, a thermoelectric module and a water reservoir	Ten hindlimbs were harvested from 7 large to giant breed dogs weighing 27-49 kg	Loads up to 4.84 kN were applied at clamps without any obvious slippage
	Klinich 2012	Sandwiched a thermoelectric module between two aluminum grips	21 samples obtained from five human placentas	No slippage

Some of the benefits associated with serrated clamps are that they are relatively inexpensive to fabricate and are easy to use, as compared with other special clamping techniques (e.g. freezing clamps). Furthermore, serrated clamps require less operator intervention and manipulation during testing. However, the compromise associated with the use of serrated clamps is that they typically induce stress concentrations at the clamped edge, resulting in permanent deformation and even premature failure. And considering the complexity of soft tissue, serrated clamps only might not be that sufficient to provide reliable fixation. Thus the authors suggest it might be necessary to combine serrated clamps with some other techniques such as freezing[7] or add some sandpaper[63], adhesive[52] or coil biding[54] that could assist clamping.

3.1.2.2 Sandpaper

Sandpaper[51, 64, 65, 66, 67, 50], filter paper[68], blotting paper[46] and neoprene paper[49] have all been used to increase the friction between the surface of the specimen and the clamps. Manoogian *et al*. combined serrated grips with sandpaper on the clamping surface to prevent slippage[63, 18, 17]. [1] Grips incorporating sandpaper generally increase the friction between the clamps and the sample without imposing extreme deformation. However, slippage may occur prior to failure as strain increases. In addition, for thick specimens, even if the sample is compressed tightly, internal slippage may occur, i.e., internal laminae may slip when loaded. Selected sandpaper grips are presented in Table 3.1.

3.1.2.3 Adhesive

Glue has been used in conjunction with clamping in efforts to reduce sample slippage at lower applied clamping pressures. [69, 52, 70, 71, 72]. For example, Soden and Kirshaw found that movement within grips could be reduced by coating the ends of specimen with Eastman's 910 adhesive and adding glue to plastic plates between small metal clamps[52]. Selected examples of the adhesive technique are presented in Table 3.1.

Unfortunately, techniques incorporating glue are vulnerable to the same issues observed with

[1] Shi *et al* proposed the peak-to-peak styled serrated grips in 2012, thus the authors assumed that Manoogian still used peak-to-valley styled serrated grips.

grips incorporating sandpaper. Both methods only operate on the superficial surfaces and do not control the sample core [55]. The tissue sample may appear less strong as the load bearing contribution of the inner fibers is compromised by slippage. In addition, it can be difficult to prevent adhesive from spreading onto the specimen, which can convolute efforts to determine mechanical properties. Moreover, water in soft tissues can make it challenging to apply adhesives exclusively to the surface of the specimen.

3.1.2.4 Winding

Another technique employed to secure the specimen within clamps involves binding the ends of the specimen with copper wires or thread[73, 74, 54, 75]. For example, Benedict *et al*. [76] wound the ends of a specimen for the first 1/2 inch with copper wire in coil fashion. They claimed that slippage was minimized but did not report the slippage rate. While in Walker *et al.*'s paper, they reported that 11 out of 30 specimens failed in the gage region, while the rest either failed at clamps or slipped. Despite the fact that winding could reduce deformations produced by high compression at the ends, the problem of inner fiber slippage remains. Additionally, the reported success rate is less than 40% in some studies[76]. Selected examples of the winding technique are presented in Table 3.1.

Admittedly, sandpaper, adhesive and winding assist fixing soft tissues and reduce the amount of clamping force required to secure the sample. However, only the superficial layers are guaranteed to be stressed. As such, these techniques may be most useful for thin, delicate samples where the inner fiber behavior is negligible. Considering the shortage of controlling the center of thick soft tissues, some researchers [6, 77] proposed self-tightened clamps with a wedge in the center. This method makes a cut in the center of a specimen and inserting a wedge into the cut. Thus there would be four surfaces (two surfaces between the wedge and the center layer of the specimen) contact between the specimen and the clamps and specimens, which would increase the friction.

3.1.3 Self-tightening clamps

One of the challenges of testing biologic tissues is that they are capable of large strains prior to failure. The traction between the specimen and its grips may decrease during stretching as the specimen thins in the transverse directions. Self-tightening clamps have been developed to maintain the applied traction throughout the experiment. In the early 1960s, Wright *et al*. [4] utilized serrated self-tightening clamps: Two wedge-like jaws were set inside the recess of a block with a tapered channel; when the specimen was stretched, the jaws are pulled by the specimen deeper into the tapered channel, thereby tightening the grip. Ultimately, all failures occurred at the edge of clamps because of the high stress concentration. A schematic drawing of the clamp is shown in Fig. 3.4. Woo, *et al.* first made a coronal cut at the ends of the specimen, and then inserted a stainless steel wedge piece into the cut surfaces of the specimen. Then the ends of the specimen with the wedged piece were both clamped. Thus the specimen was gripped at four surfaces(Fig. 3.5). In addition, the pivoted jaws could provide a self-tightening effect during the tensile test. In over 90% cases where ultimate strain values ranged from 9% to 13%, the failure occurred in the gage region of the specimen instead of near the grips. Contemporaneously, Svendsen and Thomson [6] presented a clamp that consisted of an inner plate with a conic projection and an outer plate with a mating recess. The specimen end would be drawn into the outer plate through a hole bored coaxially with the recess. The projection of the inner plate would be forced into the specimen to provide firm compression. The inner sides of the clamps were sandblasted to optimize friction. This clamp is shown in Fig. 3.6.

Self-tightening clamps are generally reliable; some of the clamps achieved 100% success rate; however, the difficulties associated with manufacturing the clamps and manipulating the specimen may make this approach impractical for some applications. Selected self-tightening clamps are presented in Table 3.1.

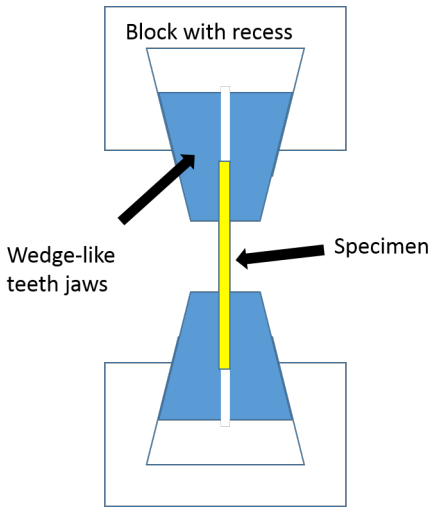

Figure 3.4: Schematic drawing of self-tightening clamps proposed by Wright[4]

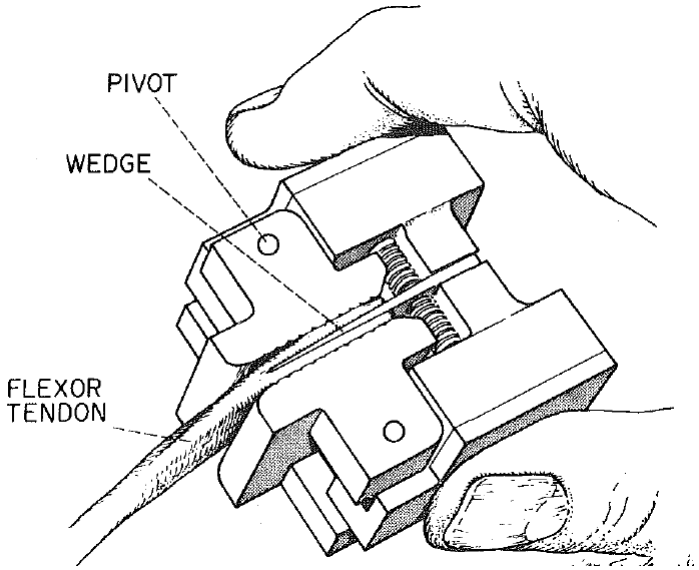

Figure 3.5: Self-tightening clamps proposed by Woo *et al*, reprinted with permission from [5]

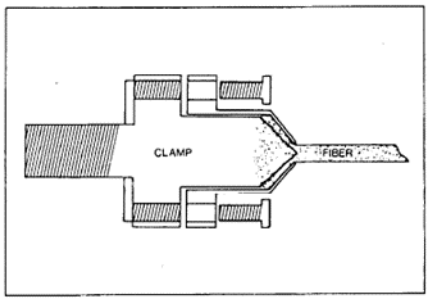

Figure 3.6: Self-tightening clamps proposed by Svendsen, reprinted with permission from [6]

3.1.4 Alter mechanical properties of clamped region

The last major approach is to alter the mechanical properties of the clamped region to be more favorable to clamping. While there are several proposed methods, this review will focus on the two most popular approaches: dehydration and freezing.

3.1.4.1 Dehydration

Haut [78] proposed a method wherein the gripped portion of the specimen was first air-dried to increase its strength and then wrapped with masking tape. The test area, or the central region, was kept moistened with saline so that the mechanical properties would not change. Ker *et al*. and Smith *et al*. also used this method [79, 56, 80] and observed that the thickness of the specimen was reduced, making the material less flexible, which results in less stress transfer [81].

It has been shown that air drying the ends of samples can decrease the frequency of failure near the grips since Wang reported over 90% success rate[56]; however, this technique may also affect the test region. Thus the results may not reflect the true mechanical behavior of specimens. Further, if the test is performed in a hydrated environment, such as a saline bath, the dehydrated parts would potentially re-hydrate, increasing the likelihood of slippage. Lastly, this approach does not mitigate potential problems associated with stress concentrations at the transition area between dry and wet [55]. Selected examples of the dehydration technique are presented in Table 3.1.

3.1.4.2 Freezing

Two techniques have become common for freezing the ends of the sample: cryogenic and thermoelectric clamps. Since the work of Riemersma and Schamhardt, cryogenic clamping has been considered a gold standard for mechanical testing of soft tissues under high tensile load. The principle behind the cryogenic technique is applying low temperature fluid (e.g. liquid nitrogen[59, 47] or carbon dioxide[7]) to freeze the clamped ends of the specimen. Doing so increases the friction coefficient between the clamps and the specimen, thus reducing compression. The fluid runs through the channels machined on the clamping blocks to freeze the ends of a specimen [7], as shown in Fig. 3.7. Since only moderate pressure is applied to hold the sample, the risk for mechan-

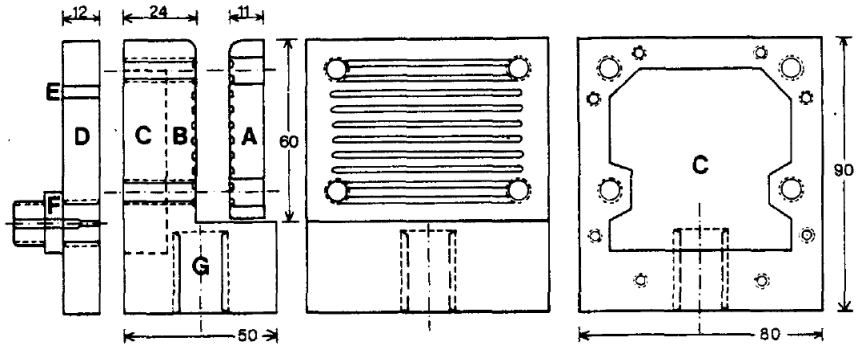

Figure 3.7: Cryogenic clamps proposed by Riemersa, reprinted with permission from [7]

ical damage is reduced and biomechanical properties in the gage region are well maintained[47]. Because freezing makes the clamped portion a solid part, displacement of the inner fibers in the frozen region can be neglected. Thus, the tensile load can be considered as evenly distributed over multiple layers of the specimen. Central to the success of this method is preventing thawing of the clamped region. This can be difficult when testing under physiological temperatures. Moreover, this technique may not be suitable for short specimens since the freezing action is difficult to constrain, and it is clearly essential to keep the test region at the relevant temperature (e.g. room temperature or 37°C). [46]. Selected examples of cryogenic clamps are presented in Table 3.1.

Thermoelectric devices, like the one shown in Fig. 3.8, present an alternative to the cryogenic approach. Cryogenic elements are replaced with a thermoelectric cooler. The temperature is detected by a sensor and regulated by a controller. This method made it possible to immerse the whole device, including the grips into a bath environment without freezing the liquid around it. Also, the grips included outer contoured surfaces suitable for gripping soft biological tissues [82]. Kiss *et al*. [8] modified a TEC VGA waterblock (MCW50-T, Swiftech, Lakewood, CA) into a device that was composed of a custom-made aluminum serrated plate, a thermoelectric module and a water reservoir. The thermoelectric module functioned as a heat pump when an electric current was applied, absorbing the heat from the cold side of the module and releasing it to the warm side, which maintained a constant temperature gradient. As voltage and current increased, the temperature increased. The water flowing in the reservoir served to dissipate heat from the warm side,

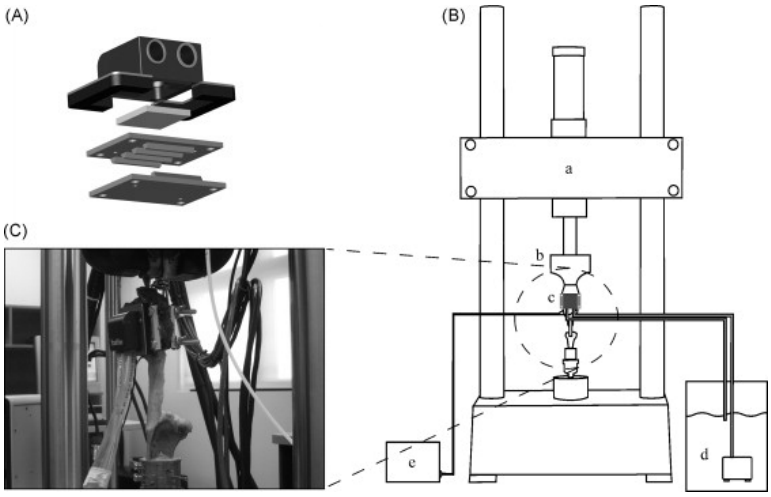

Figure 3.8: Thermoelectric clamps, reprinted with permission from [8]

which maintained the cold side at a subzero temperature. Similarly, Klinich *et al*. [83] sandwiched a thermoelectric module between two aluminum grips. Water was used as the working fluid to remove excess heat, maintaining the inner plates at -10°C.

In contrast to the cryogenic technique, the thermoelectric devices can be fully submerged in a heated bath. Moreover, once the tissue is inserted into thermoelectrically cooled clamps, no additional manipulation is required (e.g., giving a pulse of liquid CO_2 or nitrogen). However, the freezing efficiency is not as high as conventional cryogenic clamps. Some researchers report waiting up to an hour to achieve freezing with thermoelectric devices [8]. Sample degradation during this time could be a major concern. Selected examples of thermoelectric clamps are presented in Table 3.1.

Admittedly, dehydration and freezing technique are generally reliable in soft tissue fixation. However, the compromise of both techniques are that it is challenging to avoid altering mechanical properties of the test region. Additionally, among these techniques, only thermo-electric clamps have the potential to handle specimens under physiological environments, i.e., 37°. Moreover, it is quite expensive and time-consuming to apply these techniques or machine the clamps. Thus, there is a need to design and build some type of easy-to-use, economical clamps, which could also allow us to test the specimens under physiological environments.

3.1.5 Assessment

A variety of clamping techniques have been proposed over the past few decades. The success rate (specimen failure in the gage region and no observed slippage) of tensile tests using these clamps varies from 0% [4] to 100% [5, 6, 47, 57]. While the 100% success rate is an exciting result, most of these clamp designs are complicated, or use a technique that might alter the specimen's mechanical properties in the testing region. In addition, because most of these clamps are designed for thick large tissues (e.g. tendons, ligaments, fascia), many of the design benefits may not translate to applications for thinner, more delicate tissues (e.g. fibrous membrane).

3.1.6 Design of present study

The goal of this study is to propose an easy-to-use and economical clamp design for fibrous membrane tissues that provides reliable sample fixation and reduces stress concentrations at clamping sites. Moreover, it could allow for specimens to be tested under physiological environments, e.g. in a heated water bath. As proof of concept, we employed uniaxial tensile testing of a rat abdominal wall. Modified from the serrated jaw clamp [3], a new type of jaw clamp with an increased density of serrations along with needles that perforate the tissues has been developed. The introduction of needles helps to secure the clamped portions of a specimen, thereby alleviating slippage from the grip/specimen interface down to the sample core for multi-layered tissues. These clamps were 3D printed out of FullCure720, a relatively soft material, to reduce the risk of cutting tissues. This design should allow samples to be tested under physiologic conditions, submerged in fluid at 37°C. A schematic of this design is shown in Fig. 3.9.

3.2 Materials and Methods

3.2.1 Testing protocol

In this study, we performed 40 uniaxial tensile tests on dog-bone-shaped abdominal wall tissues until rupture at a strain rate of either 1% per second or 10% per second. To investigate the anisotropy of rat abdominal wall tissues, sub-sample sets were cut out along or transverse to the cranial-caudal direction. Slipped or pre-maturely failed specimens were excluded from our tissue

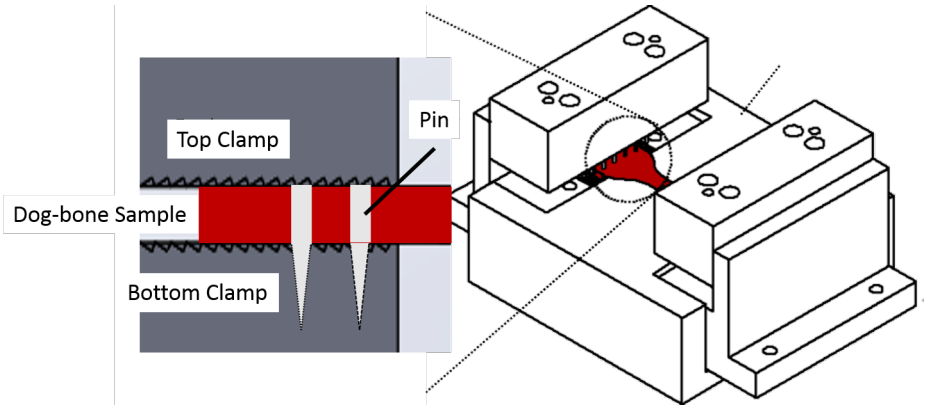

Figure 3.9: Schematic drawing of the 3D printed clamps with needles

mechanics analysis. The testing conditions and results are summarized in Table 3.2.

Abdominal wall tissue was obtained from four groups of male Sprague-Dawley rats classified as Group 1 (n=6), Group 2 (n=5), Group 3 (n=4), and Group 4 (n=4). All rats were collected from the Texas A&M University Tissue Share program. All rat abdominal wall tissues were procured immediately after death to minimize the adverse effects of tissue degradation. In order to preserve tissue during transportation, the specimens were placed in containers filled with Phosphate Buffered Saline solution (PBS), chilled with ice packs. The first two groups of tissues were tested within 48 hours of death. Groups 3 and 4 were stored in -20°C freezer for one week and then defrosted in a 37°C water bath prior to testing. All tests were performed at room temperature.

3.2.2 Specimen preparation

Specimens were cut into dog-bone shaped samples using a custom specimen cutting set (Fig. 3.10), consisting of 1) a cutting mold, 2) a cutting pad, 3) a rubber pad, 4) a cutting board, 5) a vice, and 6) a scalpel. A Teflon pad was placed between the specimen and cutting board to avoid damage to the cutting blade. [2] Guiding rods were designed to constrain the blade during the cutting process. A vice was used to apply high pressure to the blade. After pressing the tissue 3–5 times, a scalpel was used to remove connective tissues. The dog-bone samples were then immersed in a PBS solution to maintain hydration.

[2]The blades dulled easily, especially after cutting thick tissues placed on the cutting board directly.

Table 3.2: Specimen information and results

	Group 1a	Group 1b	Group 1c	Group 1d	Group 2	Group 3	Group 4
Sample size (n)	5	3	8	3	4	10	7
Orientation	Along	Transverse	Along	Transverse	Along	Along	Along
Handling	Tested within 48 hrs	Tested within 48 hrs	Tested within 48 hrs	Tested within 48 hrs	Tested within 48 hrs	Frozen 1 week	Frozen 1 week
Strain rate	1%/s	1%/s	10%/s	10%/s	1%/s	10%/s	1%/s
Success rate	60%	66%	0%	0%	100%	90%	100%
Mean UTS (std) [MPa]	0.1265 (0.0439)	0.1143 (0.0678)	N/A	N/A	0.2514 (0.0366)	0.2448 (0.1236)	0.3105 (0.1166)
Mean Stretch ratio (std)	1.5439 (0.1589)	1.3942 (0.0776)	N/A	N/A	1.7840 (0.0546)	1.3245 (0.0752)	1.3839 (0.0902)

Considering the size of the abdominal wall tissues, design of the dog-bone punch was modified between groups to maximize efficiency and harvest as many sub-samples as possible. During the cutting process and ensuing experiments it was found that those specimens cut using the punch for Group 1 were too narrow. Consequently, cutting defects could lead to deviations in the testing results; hence, a larger cutmold was designed and used to cut abdominal wall collected from large rats. Cutmold 3 was also designed for rat abdominal wall tissues collected from smaller rats. Note all the tissues were collected from Tissue sharing program, the authors did not have control on the size of rats. Cutmold 1(Fig. 3.11) is used for samples in group 1, cutmold 2(Fig. 3.12) is used for samples in group 2 and cutmold 3(Fig. 3.13) is used for samples in group 3 and 4.

Specimens collected from Group 1 rats were sorted into four subgroups: 1) Group 1a for specimens cut along cranial-caudal direction and tested under 1% per second; 2) Group 1b for specimens cut transverse to the cranial-caudal direction and tested under 1% per second; 3) Group 1c for specimens cut along cranial-caudal direction and tested under 10% per second; 4) Group 1d for specimens cut transverse to the cranial-caudal direction and tested under 10% per second. In Group 2, four samples(Fig. 3.15) were cut along the cranial-caudal direction and tested at a

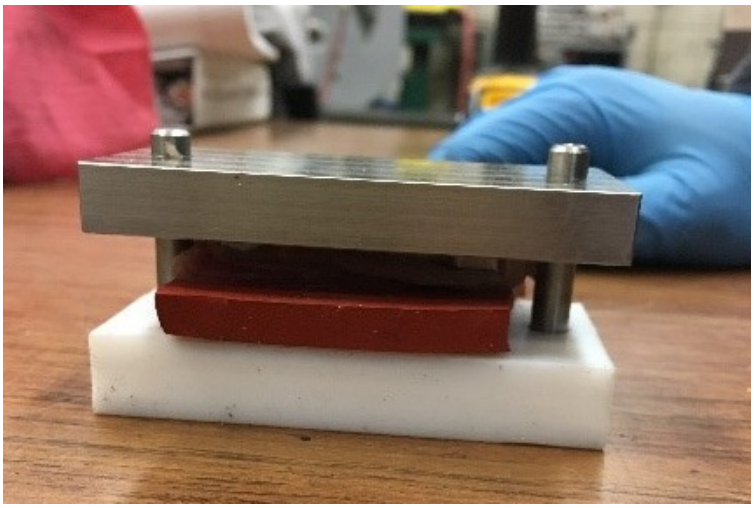

Figure 3.10: Specimen cutting set

Figure 3.11: Cutmold for specimens in Group 1

Figure 3.12: Cutmold for specimens in Group 2

Figure 3.13: Cutmold for specimens in Group 3 and 4

Figure 3.14: Specimen in Group 1

strain rate of 1% per second. In Group 3, ten samples(Fig. 3.16) were cut along the cranial-caudal direction and tested at a strain rate of 10% per second. In Group 4, seven samples(Fig. 3.16) were cut along the cranial-caudal direction and tested at a strain rate of 1% per second. Average ultimate tensile strength (UTS) and corresponding stretch ratio was calculated for all non-slipped specimens.

Group 1a (fresh, cut along cranial-caudal direction, tested under 1% per second) and Group 4 (frozen for one week, cut along cranial-caudal direction, tested under 1% per second) were compared to evaluate effects of freezing on mechanical properties. Group 3 (frozen for one week, cut along cranial-caudal direction, tested under 10% per second) and Group 4(frozen for one week, cut along cranial-caudal direction, tested under 1% per second) were compared to evaluate the effects of loading rate on mechanical properties. A two-tailed student's t-test was used to evaluate

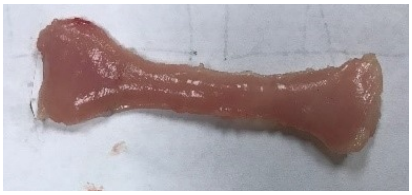

Figure 3.15: Specimen in Group 2

Figure 3.16: Specimen in Group 3

significance with threshold set at $\alpha = 0.05$. The null hypothesis is that the mean UTS between the two groups are the same or the mean stretch ratio at UTS between the two groups are the same.

3.2.3 Specimen alignment

In order to minimize the adverse effect of shear due to specimen misalignment, custom designed alignment jigs with a recess on the sample plane were used to provide consistent and convenient alignment during the clamping procedure. Clamps were placed at the two sides of the alignment jig. Then a specimen was placed on top, within the recess of the jig.

3.2.4 Clamping design

Screw-tightened, 3D printed serrated clamps were used in the design. The pitch of the serrations of the clamps was 0.02 in. (50 serrations per inch) with the indentations having a depth of about 0.008 in., at an angle of 27°on one side and 63°on the other side, as shown in Fig. 3.17. Preliminary tests were performed on serration densities of 10 teeth per inch, 20 teeth per inch, and 50 teeth per inch. The results showed a higher serration density led to less slippage. Clamps were printed on a 16 micron resolution 3D printer (Stratasys, Objet Eden 260VS, Eden Prairie, MN) with FullCure720 material. Printing time for each pair of clamps took less than 30 minutes at a

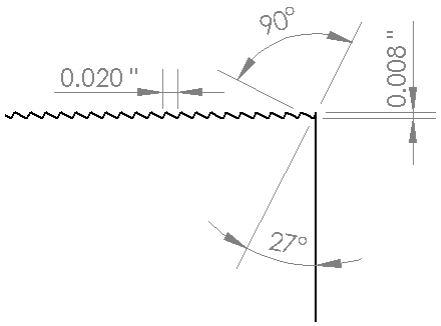

Figure 3.17: Dimension of teeth of clamps

material cost of $10–$20. In contrast, stainless steel clamps of comparable geometry take on the order of a 24 hour turnaround with incurred costs of upwards of $400 accounting for materials and labor. The resolution of the available printer limited the serration density to 50 teeth per inch. Twelve stainless steel needles were split into two rows with 0.1 in spacing and press fit into holes in the top clamp. The distance between the first row of needles to the front surface of the clamps was 0.08 in. These needles perforated the specimen as the clamp screws were tightened.

3.2.5 Success criteria

A successful test is defined as: (1) failure occurs in the gage region Fig. 3.18 and (2) no slippage is observed. Marking samples with ink near the clamping site has been previously employed to investigate sample slippage; however, details regarding how the ink markings were analyzed are generally lacking.

In this study, India ink was used to mark clamping sites to check slippage. Videos were taken on one side of the specimen for these tests and played back to inspect the slippage based on the ink. The camera used for recording is Canon VIXIA HG20, 3.3 MP. The stress-strain response of each specimen was analyzed for anomalous changes(an example is shown in Fig. 3.19, circled in red), which could be evidence of potential slippage on the side that was not imaged, or defects instigated by the sample preparation process. To be conservative, if no slippage was observed in the video verification of the ink, but a sudden jump was found in the stress-strain curve, then that test was considered unsuccessful *due to possibility of slippage*. Second, rupture at the clamps instead of

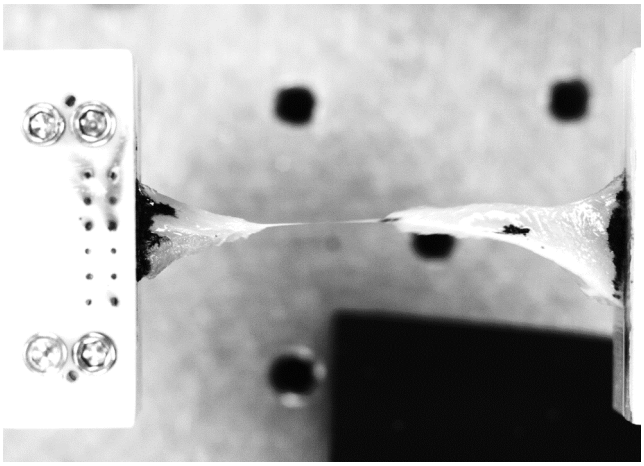

Figure 3.18: Specimen fail in the gage region

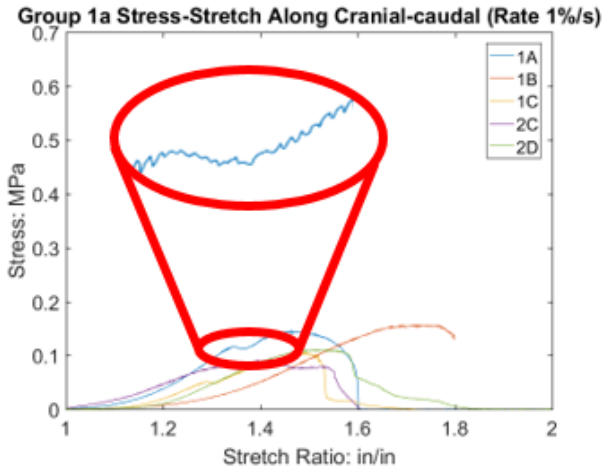

Figure 3.19: Stress-strain curve of specimens in Group 1a

the gage region due to stress concentration may not reflect the true mechanical properties of soft tissues and is considered unsuccessful as the second success criterion requires sample failure in the gage region.

3.2.6 Experimental setup

The experimental setup was a custom designed biaxial mechanical testing system. The system consisted of four servo-controlled linear actuators (Kollmorgen AKD P00306, Radford, VA) mounted on a horizontal breadboard (Newport SG-44-2, Irvine, California). The system was op-

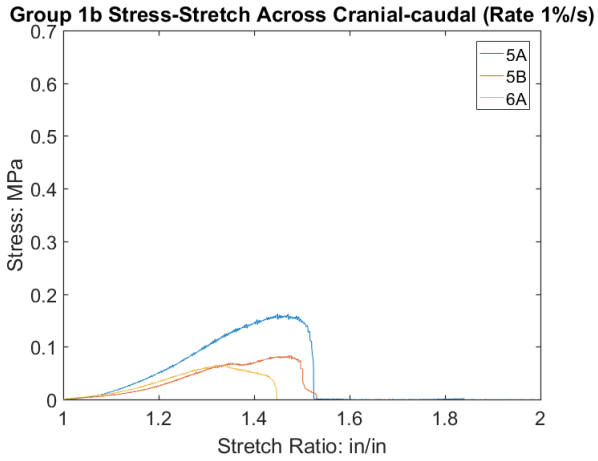

Figure 3.20: Stress-strain curve of specimens in Group 1b

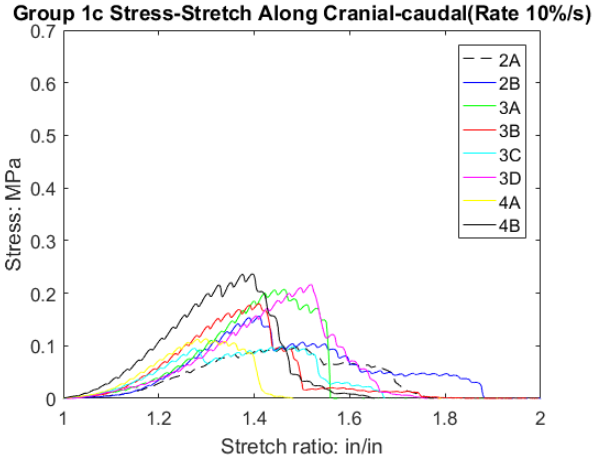

Figure 3.21: Stress-strain curve of specimens in Group 1c

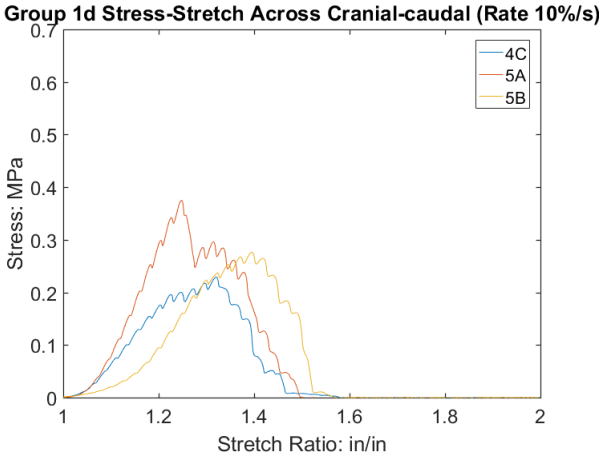

Figure 3.22: Stress-strain curve of specimens in Group 1d

erated with a multi-axial digital servo-controller (McGaw Technology, MTI Express, Lakewood, Ohio). Specimens were attached to two linear actuators , one held stable and the other drove the specimen until failure. Each linear actuator was coupled with a linear variable differential transformer (LVDT), which was used to measure the displacement between the grips. A 10 lbf (4.54 kg) uniaxial tension/compression load cell (Futek, LSB210, Irvine, CA) was used to measure the load.

3.2.7 Clamping torque

Preliminary studies showed clamping torque is important in balancing stress concentration and slippage. However, limited literature was found [84] quantifying it. In the present study, a dial torque-measuring wrench (McMaster Carr, 5718A42, Atlanta, GA) was used to quantify clamping torque to the specimen. In this study, a specified torque determined from a preliminary study was applied to each group of specimens. We initially started at 1.5 in*lb (0.17 N*m) for samples tested under both 1% and 10% per second(Group 1 and 2). After realizing that this might not be sufficient, we tuned the torque to 2.5 in*lb (0.28 N*m)for specimens tested under a 10% per second strain rate(Group 3), which achieved a 90% success rate. We increased torque to 3.0 in*lb (0.34 N*m) for specimens tested at the 1% per second strain rate(Group 4), which achieved a 100% success rate.

3.3 Mathematics

The stretch ratio, λ, of the specimen is defined as the ratio of the instantaneous distance between the grips, $\ell(t)$, and the original distance between the grips, $\ell(0)$ also referred to as the gage length, which is measured by calipers. The instantaneous distance is defined as $\ell(0)$ plus $x(t)$, the displacement of the grip experimentally measured by an LVDT, i.e.,

$$\lambda(t) = \frac{x(t)}{\ell(0)} + 1 = \frac{\ell(t)}{\ell(0)} \tag{3.1}$$

with

$$\ell(t) = \ell(0) + x(t) \tag{3.2}$$

1st Piola-Kirchhoff stress σ (force per initial cross-section area) is used for convenience. The stress is calculated from the measured axial force $\vec{F}$ using the following formula;

$$\sigma(t) = \frac{|\vec{F}(t)|}{A(t=0)} = \frac{|\vec{F}(t)|}{w\delta}. \tag{3.3}$$

where w and δ are the width and thickness of the specimen prior to testing respectively.

3.4 Results

Of the 40 uniaxial tensile tests performed, all ruptured in the gage region and no obvious slippage was observed in the India ink inspection. The stress-strain curves of fifteen specimens showed an anomalous change. These were considered as non-successful tests in the success-rate counts. The stress-strain curves show a non-linear response from the rat abdominal wall tissues for both loading rates. Orientation, handling conditions, strain rate, success rate, calculated UTS, and calculated stretch ratio are tabulated in Table 3.2.

In Group 1, specimens were secured with 1.5 in*lb (0.17 N*m) of clamping torque. In the stress-strain responses, the stress-strain responses of specimens tested at a 1% per second strain rate, showed two possible slippage events in samples cut along the cranial-caudal direction(Fig. 3.19) and one possible slippage event in specimens cut transverse to the cranial-caudal direction(Fig. 3.20). The stress-strain curves of all the specimens in Group 1 tested under 10% per second strain rate showed anomalous changes (Fig. 3.21 and Fig. 3.22). No external sign of slippage was observed. We suspect the way we cut the sample compromise the tissue. We treated these as unsuccessful tests. The average ultimate tensile strength (UTS) for for the non-slipped specimens cut along cranial-caudal direction and tested under 1% per second strain rate is 0.1265 MPa with corresponding average stretch ratio of 1.5439. The average UTS for for the non-slipped specimens cut transverse cranial-caudal direction and tested under 1% per second strain rate is 0.1143 MPa. The corresponding average stretch ratio is 1.3942.

In Group 2, specimens were secured with 1.5 in*lb (0.17 N*m) of clamping torque. In the stress-strain responses(Fig. 3.23), no sudden jumps were observed, leading to a 100% success

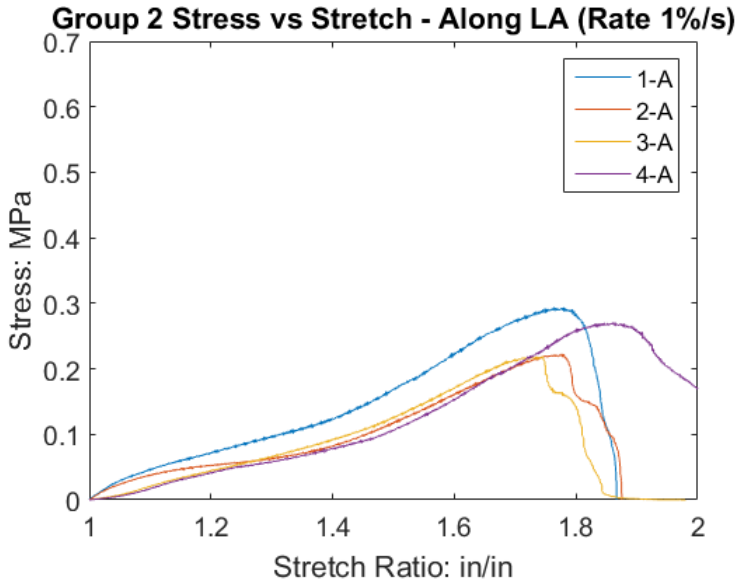

Figure 3.23: Stress strain curve of specimens in Group 2

rate. The average UTS was found to be 0.2514 MPa with corresponding average stretch ratio of 1.7840.

In Group 3, specimens were secured with 2.5 in*lb (0.28 N*m) clamping torque. In the stress-strain responses(Fig. 3.24), one specimen showed a sudden jump, leading to a success rate of 90%. The average UTS was found to be 0.2448 MPa with corresponding average stretch ratio 1.3245.

In Group 4, specimens were secured with 3.0 in*lb (0.34 N*m) of clamping torque. In the stress-strain responses(Fig. 3.25), no sudden jumps were observed, leading to a 100% success rate. The average UTS was found to be 0.3105 MPa with corresponding average stretch ratio 1.3839.

3.4.1 Mechanical properties of rat abdominal wall tissue

3.4.1.1 Loading Rate

The UTS and corresponding strain in group 3(frozen for one week, cut along cranial-caudal direction, tested under 1% per second) was, on average, smaller than group 4(frozen for one week, cut along crania-caudal direction, tested under 10% per second). The difference of UTS between these two groups is not significantly different(p=0.29). The corresponding strain between these

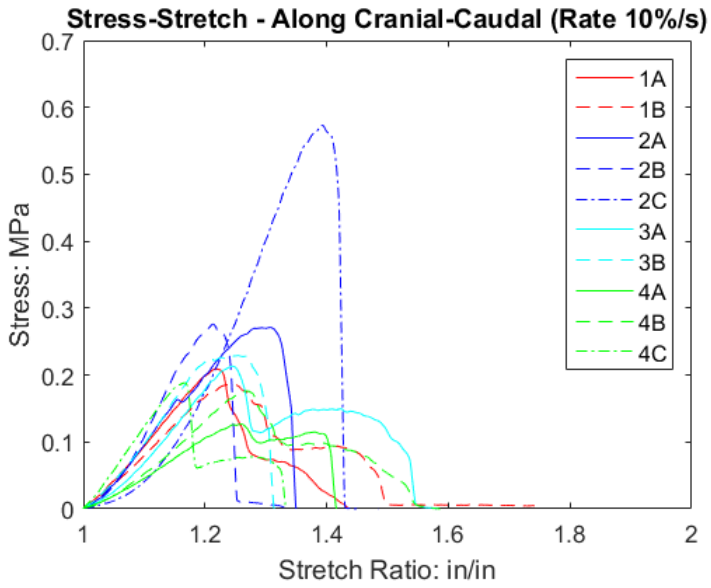

Figure 3.24: Stress-strain curve of specimens in Group 3

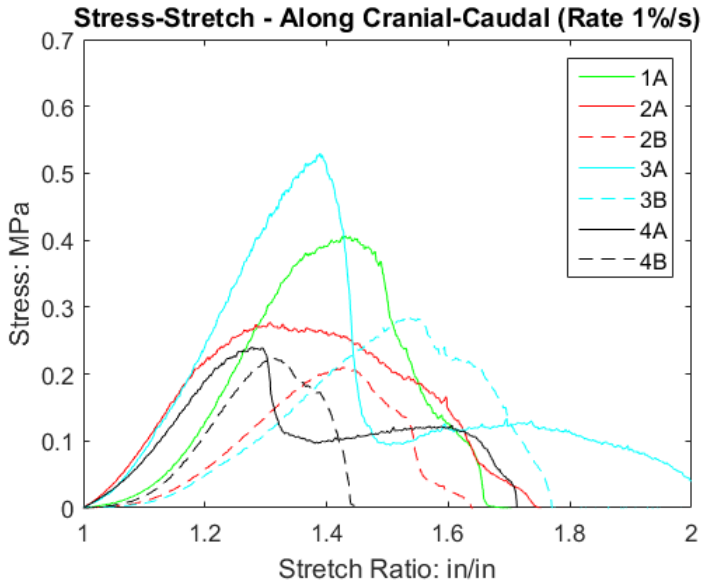

Figure 3.25: Stress-strain curve of specimens in Group 4

two groups were not significantly different (p=0.16).

3.4.1.2 Anisotropy

Ultimate tensile strength (UTS) and corresponding strain was, on average, smaller in Group 1b (transverse to cranial-caudal direction, n=2) than Group 1a (along cranial-caudal direction, n=3), but the difference was not significant (p=0.84 for UTS, and p=0.26 for strain). The low sample size is a limitation.

3.5 Discussions

The goal of this study was to design a novel clamping mechanism for uniaxial tensile testing of biological tissues, namely, rat abdominal wall. As a byproduct of validation studies, the ultimate tensile strength and corresponding stretch ratio of the rat abdominal wall muscles were calculated. The 3D printed serrated clamps with needle fixtures attached demonstrated an overall reliability in fixing rat abdominal wall tissues in this study. The clamping system proved quite easy to operate and could potentially be used in a wide array of testing environments (for example, a 37°C saline bath).

The needle clamp is promising in securing the specimen, provided appropriate torque is determined through preliminary tests. We initially applied 2.5 in*lb (0.28 N*m) to specimens tested under 10% per second strain rate (Group 3). After realizing that there was sill a 8% possible slippage rate, we decided to go to a higher torque. Thus in Group 4, a clamping torque of 3.0 in*lb (0.34 N*m) was selected resulting in a 100% success rate. Thus, we recommend the torques used in group 4 (in*lb) for reliable clamping.

According to the authors' practice, the width (d_2) of the ends of the specimens should always be narrower than the distance (d_1) between the out-most two needles, as shown in Fig. 2e. We infer that the needles help fix the center core to prevent slippage; however we did not quantify potential slippage of the core.

Based on the observations made when testing Group 1 at a strain rate 10% per second, it is important to consider the geometry of the specimens employed when conducting mechanical

tests. In determining an appropriate sample geometry the micro-structure of the tissue must be considered. Disruption of important load bearing structural complexes within the tissue could significantly affect the results. For tissues similar in micro-structure to the rat abdominal wall tissue we studied as part of our proof-of-concept, we recommend the geometry used in groups 3 and 4.

3.5.1 Comparison with other clamps

Metal clamps with serrated teeth can cause severe damage at the clamping site, which might lead to premature failure. Yet, plastic clamps with serrated teeth might not be sufficient on their own to secure the specimens. Thus, in our design, needles are introduced to assist plastic clamps in securing specimens. With the assistance of needles, we might be able to achieve the fixation of tissues with less stress applied from the serrated clamps. Compared with freezing or dehydration techniques, our design does not require altered mechanical properties of soft tissues. Thus, operation is much easier. Fabrication with 3D printing has the benefit of reduced manufacturing time and financial cost.

3.5.2 Limitations & future work

One of the major motivations behind introducing needles is to prevent sample core slippage since some tissues could be very thick. So far, we still lack an adequate technique to evaluate the sample core slippage during experimentation.

In the experiments, only one side of the specimens was videoed and used to check slippage. Given the thickness of the sample, it would be worthwhile to evaluate both sides in a future study. Some specimens exhibited an anomalous change in the stress-strain curve even though there was no clear sign of slippage in our video analysis. We suspect that this might be caused by slippage on the other side of the tissue, internal failure, or some defects of the specimen itself. To be conservative, we treated these cases as unsuccessful tests. Further studies will be involved in checking slippage from both sides.

Due to the limit sample size, we only investigated a couple of clamping torques. It is necessary

to conduct a more systematic study to investigate which clamping torque could achieve a higher success rate.

The design of this novel clamping mechanism was motivated by the need to evaluate the mechanical properties of rat abdominal wall tissues. It is acknowledged that there is a wide variety of soft tissues, each potentially possessing unique mechanical properties. Rat abdominal wall muscles are composed of rectus abdominis, external oblique, internal oblique, and transversus abdominis. Due to the limitation of the size, in this study, we cut the tissue macroscopically. It is therefore necessary to evaluate the reliability of this clamping technique for the different types of abdominal wall as well as other varieties of soft tissues, such as skin, in the future.

One of the most widely used clamps with serrated teeth has an angle of 60°. In this work, we adopted the design of Shi *et al*[3] in the selection of an appropriate angle - 63°. While we did not vary the teeth angle in this study, it would be a worthwhile evaluation of this clamp design. The present study only evaluated one version of needle spacing geometry i.e. each pin was spaced 0.1 in top to bottom, side to side. Altering the spacing dimensions and geometry, such as horizontally offsetting the second row, may yield differing success rates and are worth future study. In determining the stretch ratio, only global stretch ratio (determined from the grip distance) is calculated. Considering the specimen is in dog-bone shape, the stretch at the gage area should be higher than the global stretch ratio measured through grip displacement. In the design of dog-bone shape biological tissues, the ratio between the width and thickness might be considered to maintain the specimen's integrity and avoid cutting defects. To the author's knowledge, there has been limited ASTM standard developed for mechanical testing of biological tissues. In Group 1, defects may have been introduced in the sample preparation process, e.g. the width of the specimen may have been too narrow. The width of the punch was increased to avoid this potential issue in Groups 2, 3, and 4. Given the broad range of biologic tissues, future efforts to develop a catalog of appropriate sample preparation methods for the mechanical testing of specific biologic tissues or tissue classes will be a necessary precursor to the establishment of ASTM/ISO standards.

4. STRAIN MEASUREMENT OF SOFT TISSUE FROM BOTH SIDES

4.1 Introduction

4.1.1 Mechanical testing on soft tissues

Mechanical characterization of soft biological tissues is a foundation of biomechanics. A variety of soft tissues have been studied under uniaxial or biaxial loading conditions. [37, 85, 86, 87, 88, 89, 33, 90] One of the challenges in this field is to quantify the deformation under complex loading environment.

4.1.2 Strain measurement techniques

A variety of strain measurement techniques have been implemented in the mechanical testing, which include extensometer[91], video-dimension analyzer (VDA)[85, 9], optical markers tracking [33, 90, 92, 13], and digital image correlation (DIC)[41, 43].

4.1.2.1 Extensometer

Clip-on extensometers have been widely used in the strain measurement of tensile tests. Ohman *et al* employed an extensometer which is equipped with needles at both ends pinned into soft tissues to measure the elongation[91]. However, implementing of conventional extensometers for strain measurement is prohibited for mechanical testing of highly compliant soft tissues under large strain (20 100%) due to the mechanical interference between the extensometer and the soft tissues.

4.1.2.2 Video-Dimension Analyzer (VDA)

Developed by Yin *et al*[9], the Video Dimension Analyzer (VDA) technique output voltage signals "linearly proportional to the separation distance of two parallel markers"[92]. Lanir and Fung applied this technique to the strain measurement in their biaxial mechanical testing by using a pair of video cameras to independently monitor and analyze the distance between two parallel painted lines on each axis[85], as shown in Fig. 4.1. However, this technique only provides an average of extensional strain. Data about hear strain is absent.

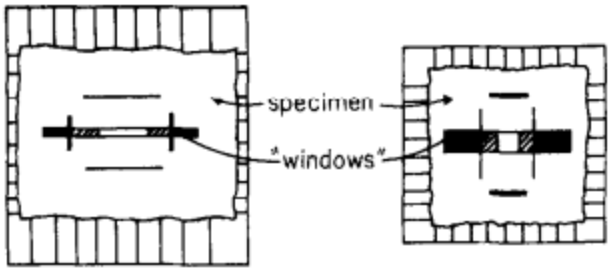

Figure 4.1: Video-Dimension Analyzer, reprinted with permission from [9]

4.1.2.3 Optical Marker Tracking

In strain measurement of biaxial mechanical testing of soft tissues, Sacks developed a tracking algorithm by setting the instensity level of the pixels corresponding to the marks at the level of 0 and those corresponding to tissues at 255. Then a 50x50 pixel image sub-region was positioned on each marker. The location of the marker was determined as the centroid of all the 0 intensity level pixels within its respective sub-region [33]. Humphrey *et al* developed a tracking algorithm to locate the center of the marker by searching through rows and columns and summing a row or column of pixel intensities. The pixel location corresponding to the maximum (light marker) or minimum (dark marker) sum is considered as the center[92], as shown in Fig. 4.2. However, this technique is limited to a small number of regions of interest. Additionally, it is time consuming to paint or glue markers to the surface of the specimens.

4.1.3 Strain measurement for multi-layer soft tissues (skin)

Skin is a continuous membrane which covers the whole body. It is valuable to study it with respect to surgical techniques and clinical potential of tissue-engineered constructs. Although skin is relatively thin, it is still composed of three main layers: 1) epidermis, the outermost layer of skin, made of closely packed epithelial cells; 2) dermis, beneath the epidermis, contains tough connective tissue, hair follicles, and sweat glands; and 3) hypodermis, which is composed mainly of loose connective and fatty tissues. Even epidermis and dermis still contains multiple layers of cells. There have been various studies about rats, rabbits or human skins [86, 93, 94, 95].

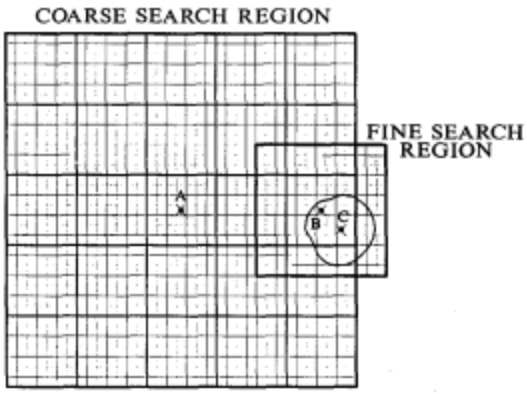

Figure 4.2: Optical marker tracking, reprinted with permission from [10]

After realizing the complexity of skin specimens, Annaidh *et al* removed adipose tissues and the epidermis layer to study a single layer of skin [96]. Griffin *et al* manually dissected off the adipose and the thin layer of deep dermis and investigated the average properties of the split-thickness skin constitutes [94]. However, some researchers tested the multi-layered skin samples without dissecting them into single layers and used the strain measured from only one side (typically the side exposed to air) to characterize the mechanical properties of the skin. [86, 93, 95, 97].

Here the authors propose that even skin is very thin, it is still a multi-layered soft tissue, or a biological composite. There is connection between different layers. Separating skin into multiple isolated samples could cause damage to the collagen fiber network, thus deviating the measured mechanical properties. Considering the complexity of thin but multi-layered soft tissues, the authors suggested that it might be necessary to consider the deformation from both sides. It is likely that the fiber orientations are different between different layers; these layers might undergo different deformation even under the same loading environment.

4.1.4 Study on deformation from both sides of rat skin samples

To the authors' knowledge, researchers tend to select the surface exposed to air that had less or no connective tissues adhered to for strain measurement. One possible reason could be that it is cleaner and easier for handling and measurement. A list of the researchers who implemented optical strain measurements in skin tissues is shown in Table 4.1. Note all of them selected the side

Table 4.1: Strain measurement of skin

Authors	Year Published	Sample	Which side used for strain measurement	Measurement Technique
Lanir, Fung	1974	Rabbit skin	the side exposed to air	VDA
Shang, Yen, Gaber	2007	Rat skin	the side exposed to air	VDA
Staloff, Rafailovitch	2008	Back of hand skin	the side exposed to air	DIC
Kvistedal, Nielsen	2009	human skin	the side exposed to air	N/A
Annaidh, Bruyere, Destrade *et al*	2012	human skin	the side exposed to air	DIC
Skilborstad, Goulbourne	2013	Bat skin	the side exposed to air	DIC, PIC
Rizzuto, Carosio, Prete	2013	mice skin	the side exposed to air	DIC

of the skin exposed to the air for strain measurement. However, the skin containes multiplayers, which could be treated as a biological composite. The hypodermis laery(inner side) might have different fiber orientation other than the epidermis layer(the side exposed to air), thus will go under a different deformation.

The objective of this research is to conduct mechanical testing on a thin but multi-layered soft tissue – rat skin and measure and compare the deformation between both sides.

According to the authors' preliminary tests, the 2D-DIC full-field technique might not be very robust for the epidermis side of skin sample due to the wrinkling and connective tissues that are hard to be removed completely. The authors decided to use the four-dots optical marker tracking method. A custom written C++ and OpenCV code is employed to track the markers and compute the deformation.

4.2 Methods

4.2.1 Subject information

Uniaxial tests were performed on rat abdominal skin which was dissected from seven male Sprague-Darwley rats. All the rats were collected from the tissue sharing program in Texas A&M University. The age was recorded in Table 4.2. Skin samples were obtained immediately after

Table 4.2: Specimen information of rat skin

Subject ID	Age (months)	Sub-samples generated
1	7	4
2	7	4
3	7	2
4	5	2
5	3	2
6	9	4
7	9	4

euthanization. Samples were shaved to remove hair. In order to preserve the tissues between the time of procurement and specimen preparation, all samples were immersed in tubes filled with phosphate buffered saline (PBS) solutions immediately after dissection and chilled with ice packs. 1 to 5 samples were stored in a -20 °C refrigerator for five weeks prior to testing. 6 and 7 samples were stored in a -20 °C refrigerator for three weeks. All the samples were thawed in a 37 °C water bath prior to testing.

4.2.2 Specimen preparation

Rectangular shaped sub-samples were cut out from rat skin subjects with scissors and a 2 x 0.5" rectangular board. The long side was across the cranial-caudal direction. Each main sample could be cut into two to four sub-samples depending on its size. All sub-samples were screened after cutting to ensure there is no obvious damage or defects that might affect the mechanical behavior. Loose connective tissues were removed as much as possible. Thus epidermis and dermis layers were preserved. Then four black beads were glued at each side of the specimen with superglue to form a 8 x 8 mm grid. Special attention was paid to the specimen during the gluing process to avoid spreading extra glue to the surface of the specimen, which could add artifacts to the mechanical behaviors of the specimen, as shown in Fig. 4.3.

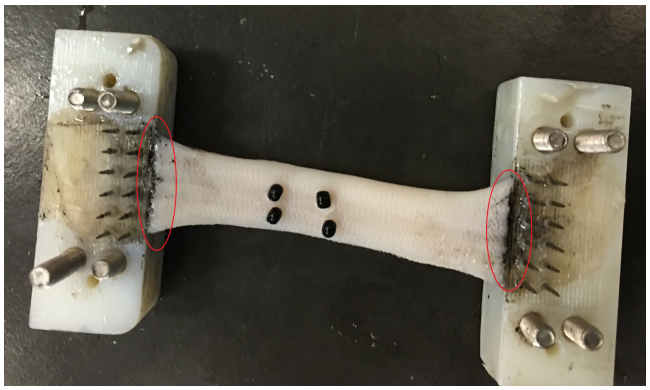

Figure 4.3: Specimen with dot glued to its surface

4.2.3 Testing configurations

The major component of the experimental setup is a custom designed biaxial mechanical testing system. The system consisted of four servo-controlled linear actuators (Kollmorgen AKD P00306, Radford, VA) mounted on a horizontal breadboard (Newport SG-44-2, Irvine, CA). Each linear actuator was instrumented with a linear variable differential transformer (Honeywell Sensotec MVL7C, Columbus, OH), which was used to measure displacement of the grip. The system was operated with a multi-axial digital servo-controller (McGaw Technology, MTI Express, Lakewood, OH). The testing system drives the specimen by moving the grip away from the opposite one at a constant velocity.

Custom made serrated clamps(Fig. 4.4) were used to minimize the slippage. India ink was used to mark clamping sites. A custom designed alignment jig was used to provide consistent clamping of the specimen, which is shown in Fig. 4.5 . Clamps were placed at the two sides of the alignment jig. Then a specimen was placed on top of the recess of the jig. The alignment jigs were designed to allow the bottom of the recess and the clamps to be in the same plane. Then specimens were placed in the recess and clamped. Then the clamped specimen was transported to the testing system and mounted to the custom made adapters attached to the linear actuators. These adapters were used to raise the specimen during the test so that the cameras mounted on the side axes could capture the images without the limitation of space, Fig. 4.6. The initial grip distance is designed

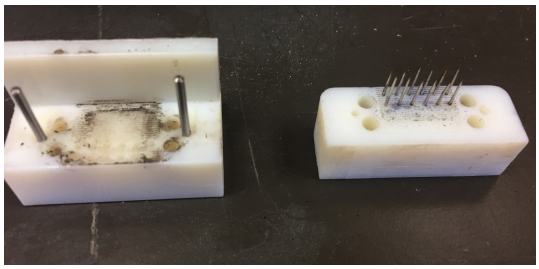

Figure 4.4: Custom-made clamps

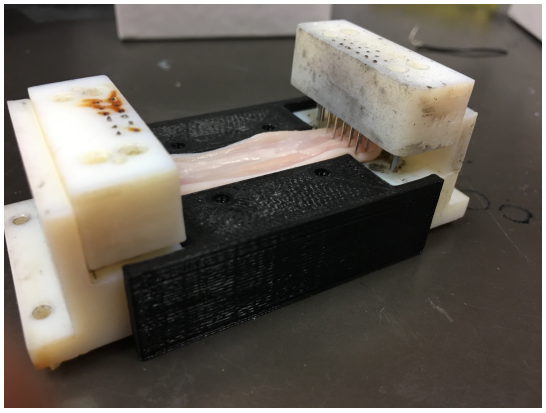

Figure 4.5: Alignment jig

as 1.5 in. After the specimen was mounted, grip distance was adjusted to avoid dangling due to the gravity of the specimen.

One linear was held stable, and the other drove the specimen to 30% stretch at a strain rate of 1%/s . The stretching axis is along the system's X Axis. Specimen deformation was measured using optical markers placed on each side of the specimen. Pre-stretch was applied prior to testing to avoid dangling of the specimen due to gravity. Note the stretch ratio was determined from the grip distance. One machine vision camera is mounted on a linear actuator at each side of the stretching axis to capture the images during the motion. The two linear actuators on the sides have been lined perpendicular to stretching axis. Thus the camera optical axis is perpendicular to the stretching axis. A schematic drawing of the system is shown as Fig. 4.7. a USB vision camera (Basler acA1300-200um, Basler AG, Ahrensburg, Germany mounted on +Y Axis at a resolution

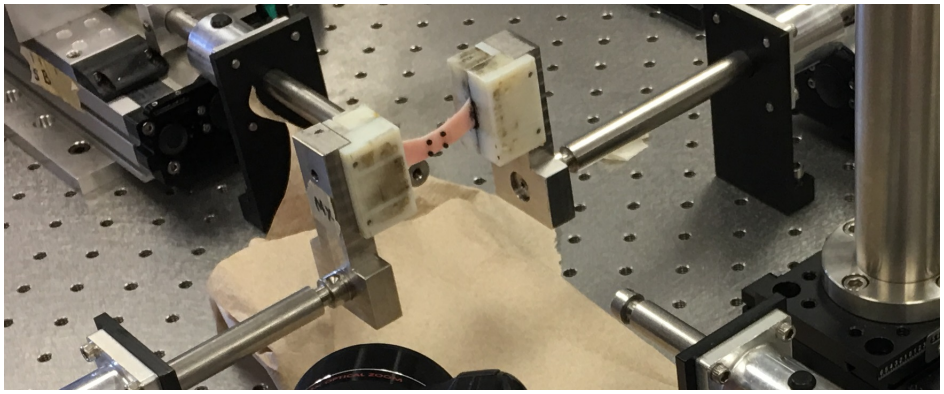

Figure 4.6: Raised fixture

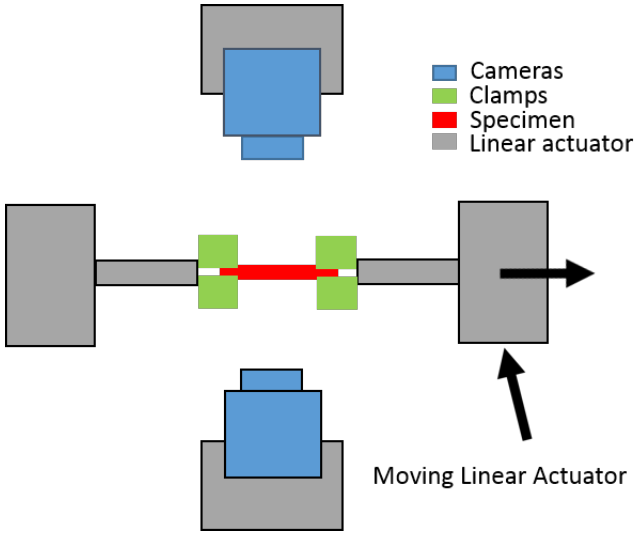

Figure 4.7: Schematic drawing of the system

of 1280x1024 and a GigE vision camera (Mako G-419, Allied Vision, Exton, PA) mounted on –Y Axis at a resolution of 2048x2048. All the tests were performed at room temperature. At the end of each test, the clamps were disassembled to check the slippage of the specimen, as shown in Fig. 4.3 (marked in red circle).

4.2.4 Strain calculation

The method described to measure strains in this paper was initially developed by Hoffman and Grigg, and Humphrey *et al*[98, 10]. The markers in this method were treated as nodes of a four

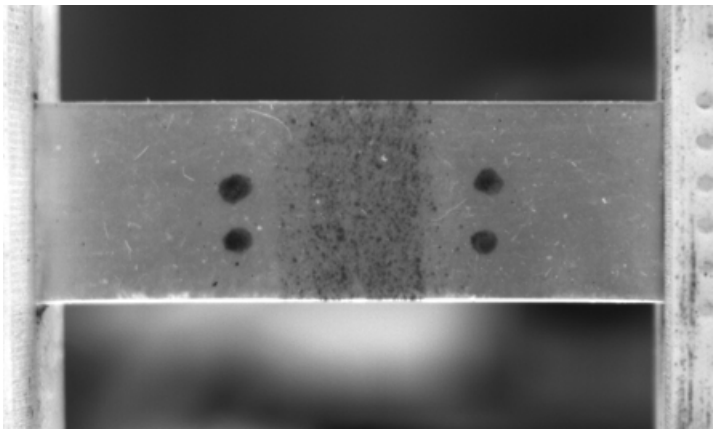

Figure 4.8: Validation image captured by Camera 1

node quadrilateral element. The shear and normal strains can be calculated from any point within the grid region formed by the four markers. The coordinates and displacement of the markers captured by the camera are mapped to an isoparametric element in another plane (square shape) using a finite element based method. There is no constraint on the geometry of the grid.

4.2.5 System alignment investigation

A preliminary study was performed with a 2 x 1.5 in semi-transparent silicone membrane with four dots painted on it to evaluate the alignment between the optical axis of the camera and the specimen, as shown in Fig. 4.8 and Fig. 4.9. 30% stretch is applied during the test. We measured the deformation from the dots with the particle tracking approach. The results are shown in Fig. 4.10, Fig. 4.11 and Fig. 4.12. By comparing the analyzed strain data from both sides, we noticed that the data were very close. Thus we decided that the alignment is acceptable.

To investigate whether the alignment between the optical axes of the cameras and the specimen has effects on strain measurement, each specimen was cut into two or four sub-samples. Every one sub-sample was placed in Group A, which had the epidermis layer(the surface exposed to air) facing Camera 1(Mako G-419, Allied Vision). Every other sub-sample was placed in Group B, which had the epidermis layer facing Camera 2(acA 1300-200um, Basler).

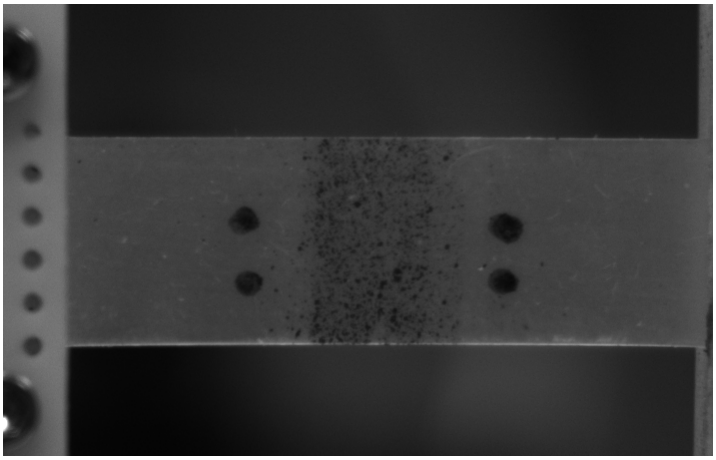

Figure 4.9: Validation image captured by Camera 2

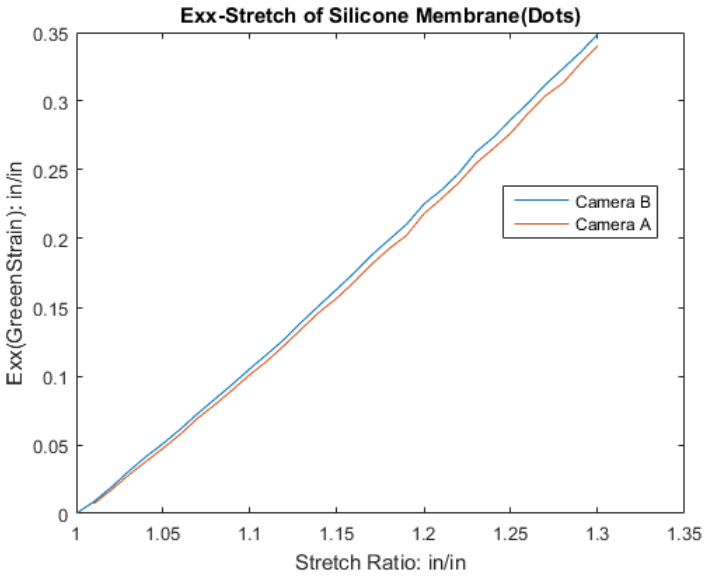

Figure 4.10: Validation results for Exx

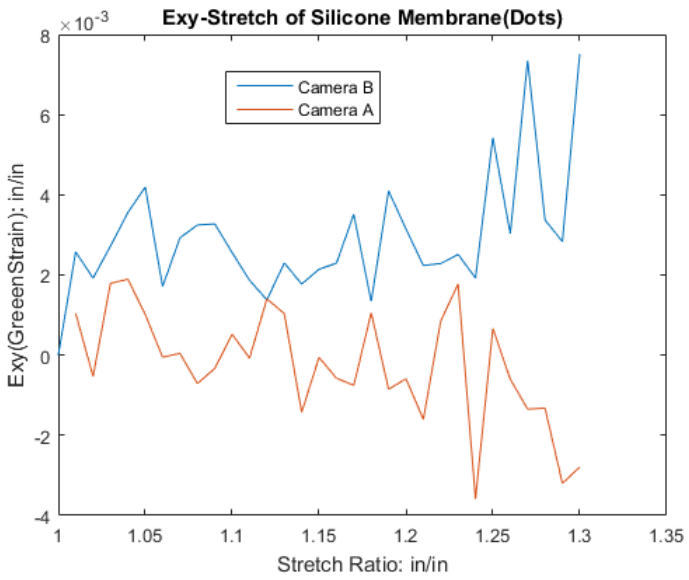

Figure 4.11: Validation results for Exy

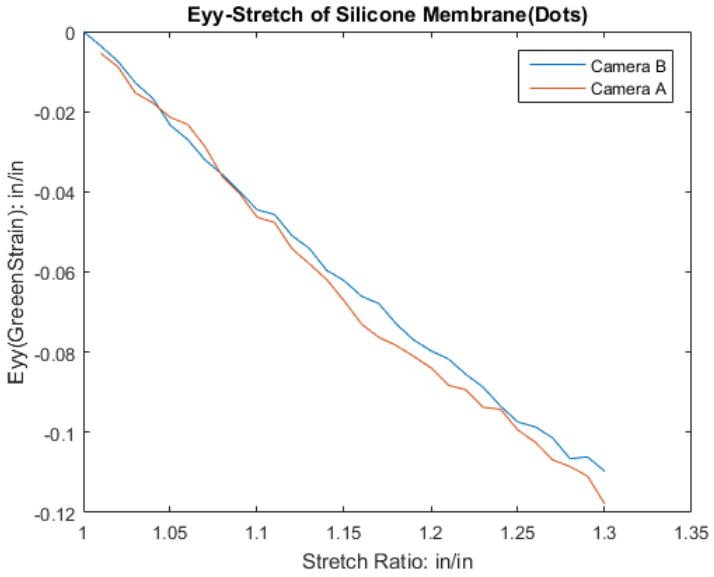

Figure 4.12: Validation results for Eyy

4.2.6 Statistics

The Exx and Eyy of epidermis layers of sub-samples in Group A(the epidermis layer facing Camera A) and those in Group B(the epidermis layer facing Camera B) were compared respectively to investigate the effects of camera-setup on the strain measurement. Similarly, this was done for the hypodermis layers.

A two-tailed t-tests were used to evaluate significance with threshold set at $\alpha = 0.05$. The null hypothesis is that the mean Exx/Eyy between the two groups are the same.

The Exx and Eyy of epidermis layers and those of hypodermis layers of sub-samples were compared respectively to investigate the difference between strain of the two sides of rat skins under the same loading environment.

A two-tailed paired t-tests were used to evaluate significance with threshold set at $\alpha = 0.05$. The null hypothesis is that the mean Exx/Eyy between the two groups are the same.

4.3 Results

Tensile tests were performed on the rat abdominal skin samples at 30% stretch ratio under 1%/s strain rate. Specimens in Group A had the epidermis layer facing Camera 1 (Allied Vision Mako G419) and specimens in Group B had the epidermis layer facing Camera 2 (Basler acA 1300-200um). The components of Green strain (Exx, Exy, Eyy) were plotted against the stretch ratio measured by grip separation for both the epidermis and hypodermis layers. The data for Exx, Exy, and Eyy of the tested specimens in each group at the last stage(30% stretch level) are tabulated in Table 4.3 and Table 4.4. The results were plotted in Fig. 4.13 to Fig. 4.24.

4.3.1 Epidermis layer of specimens

4.3.1.1 Specimens in Group A

As the stretch increased, the Green strain along the stretching direction (Exx) increased(Fig. 4.13). The average Exx at the epidermis layer at 30% stretch was about 0.32, while the standard deviation was 0.05.

As shown in Fig. 4.14, the shear strain Exy of most specimens at 30% stretch was less than

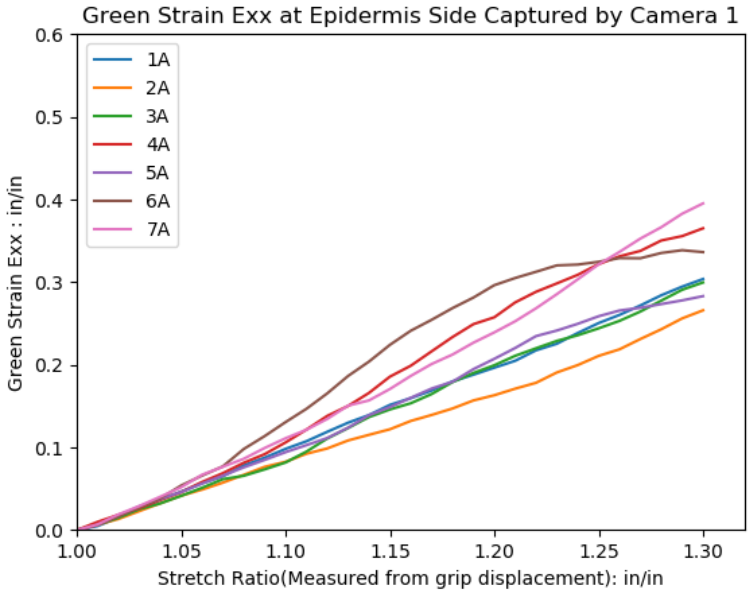

Figure 4.13: Exx of the epidermis layer of specimens in Group A

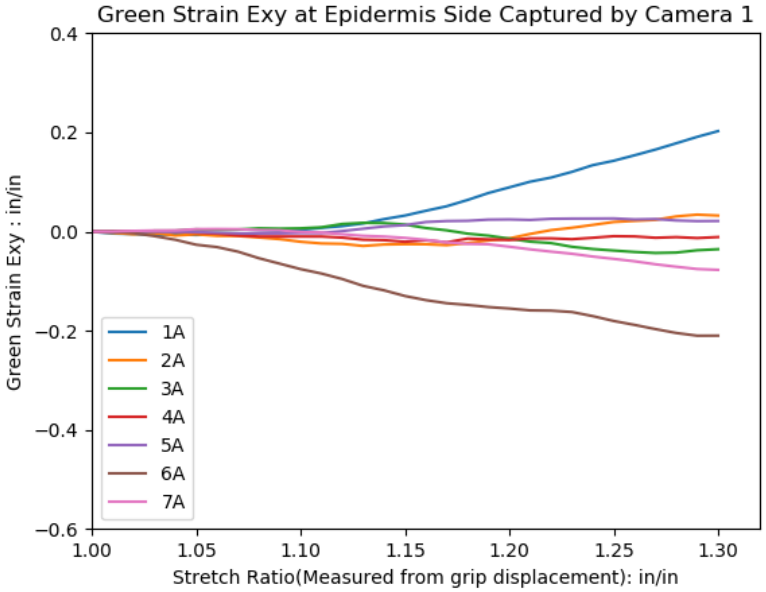

Figure 4.14: Exy of the epidermis layer of specimens in Group A

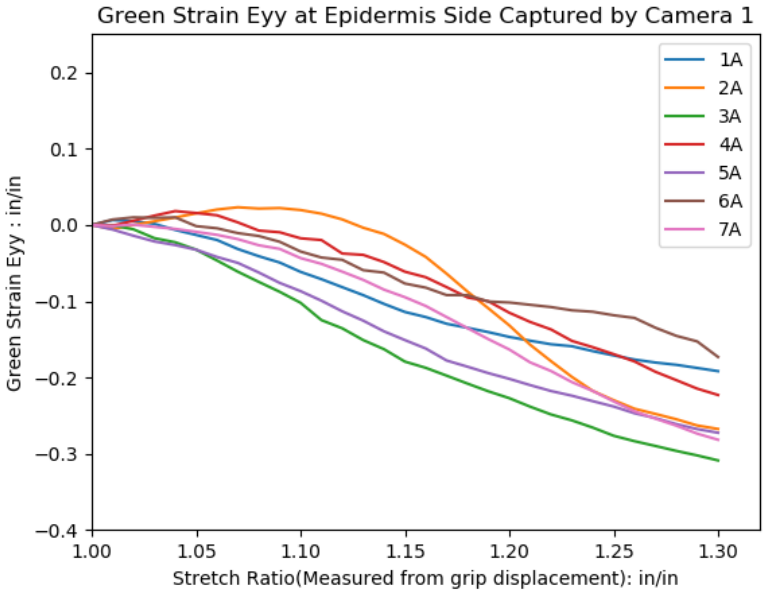

Figure 4.15: Exy of the epidermis layer of specimens in Group A

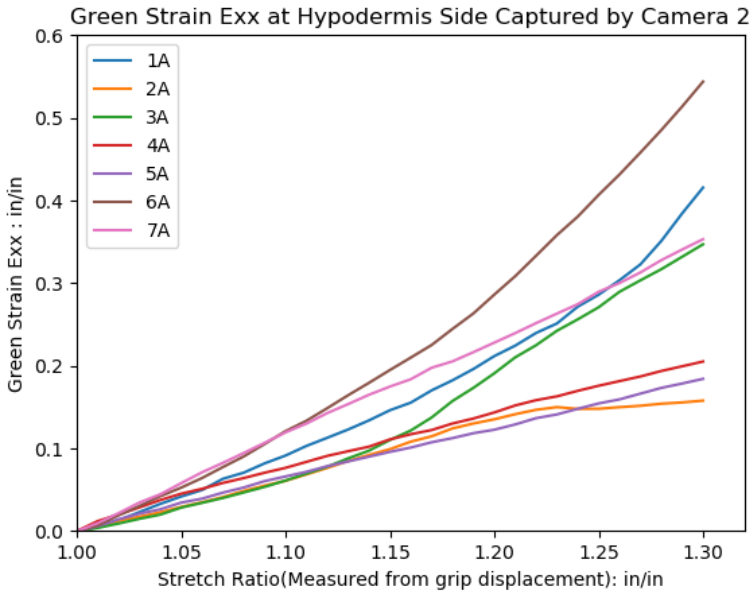

Figure 4.16: Exx of the hypodermis layer of specimens in Group A

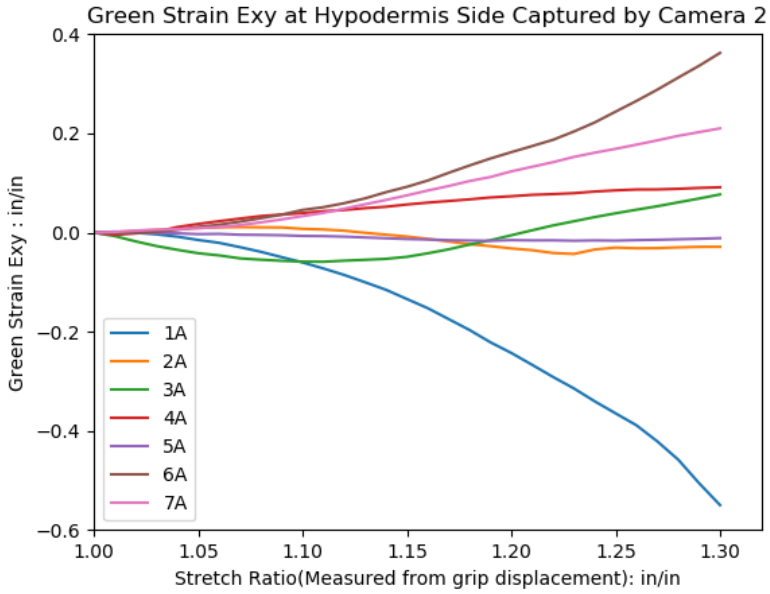

Figure 4.17: Exy of the hypodermis layer of specimens in Group A

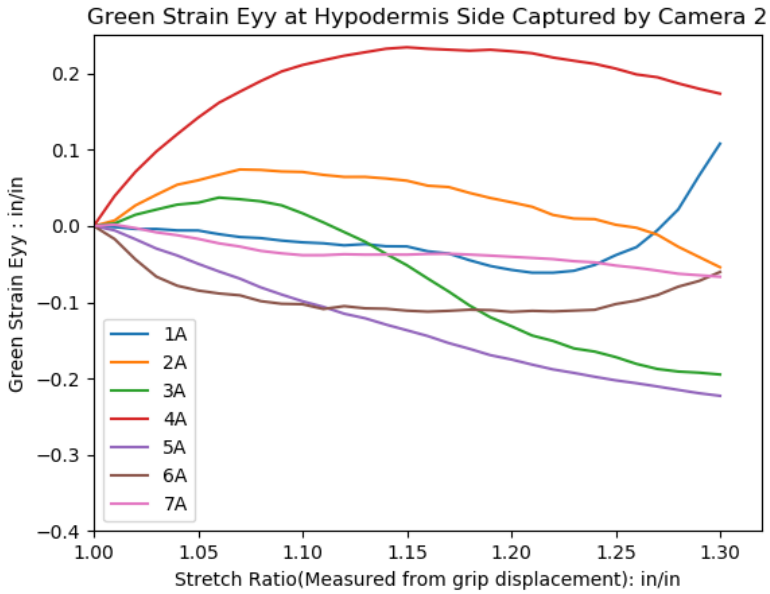

Figure 4.18: Eyy of the hypodermis layer of specimens in Group A

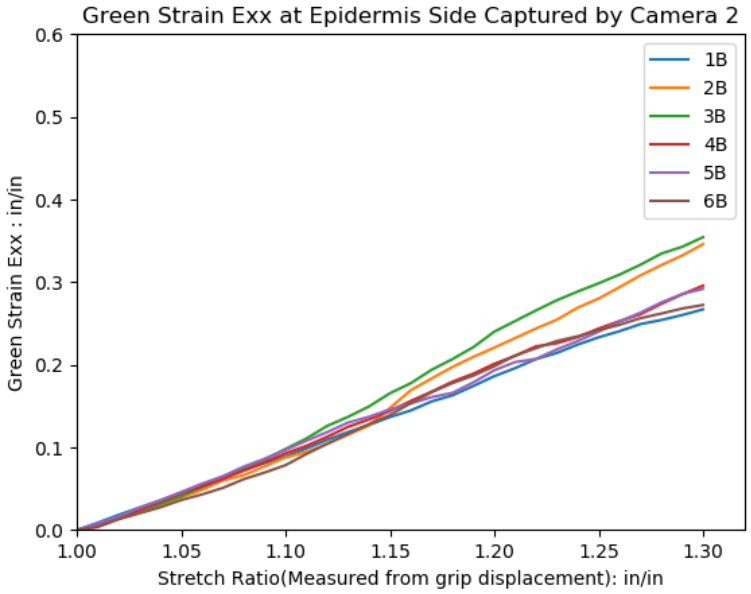

Figure 4.19: Exx of the epidermis layer of specimens in Group B

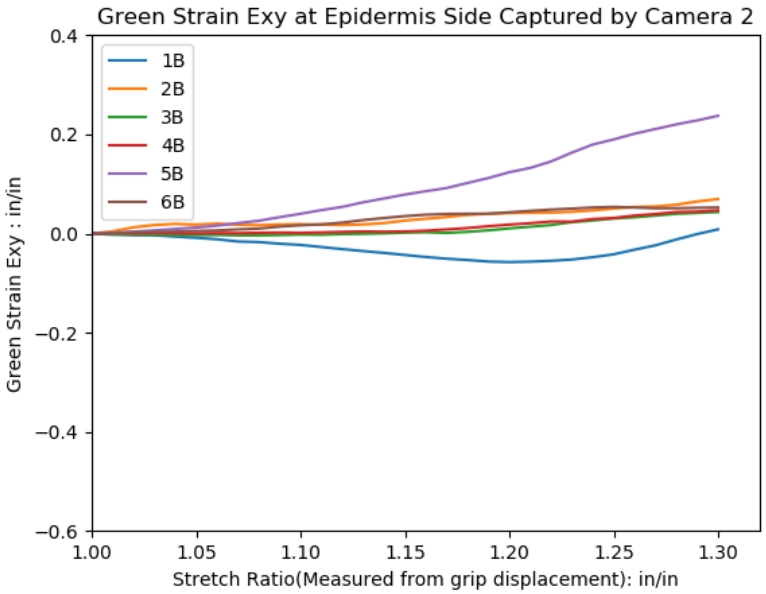

Figure 4.20: Exy of the epidermis layer of specimens in Group B

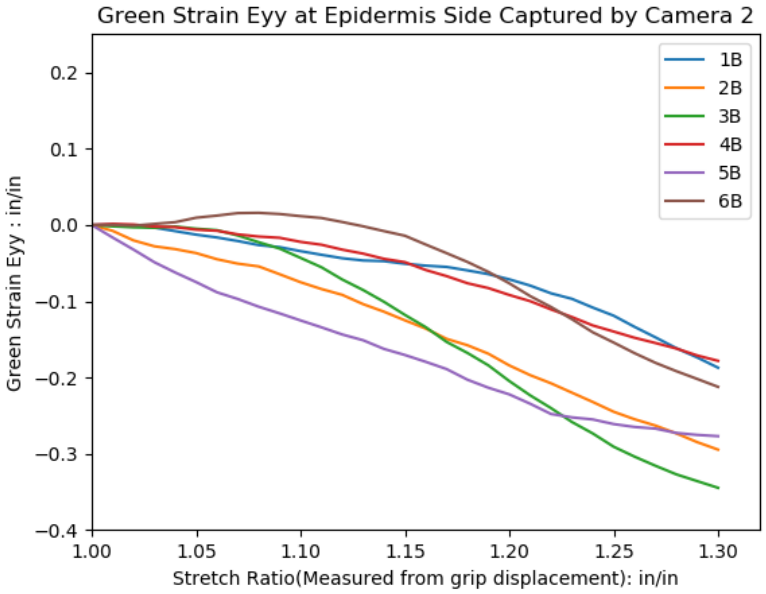

Figure 4.21: Exy of the epidermis layer of specimens in Group B

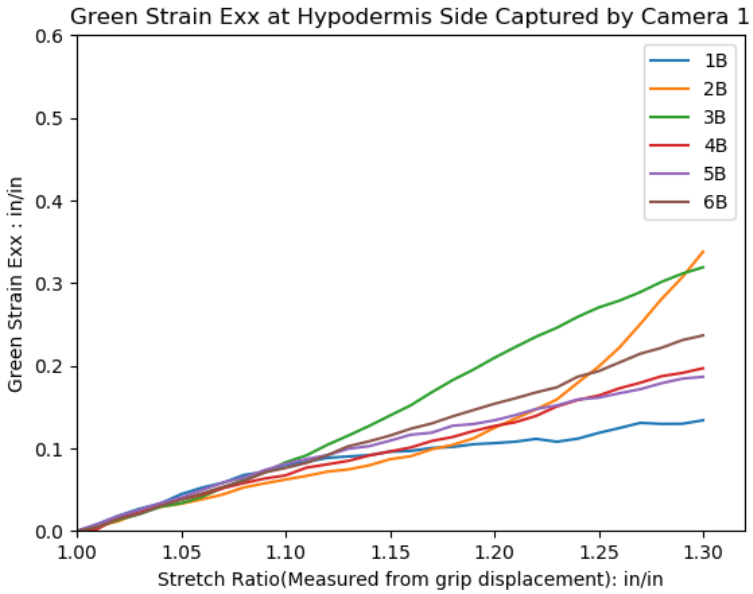

Figure 4.22: Exx of the hypodermis layer of specimens in Group B

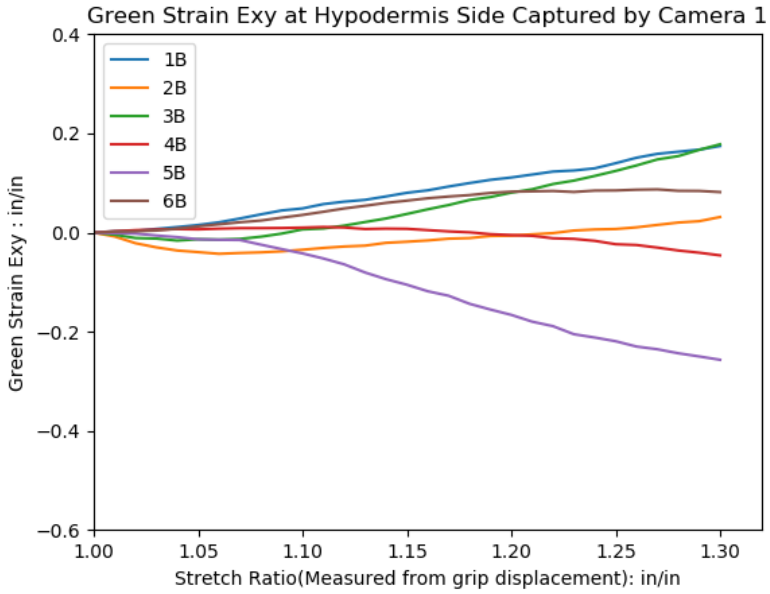

Figure 4.23: Exy of the hypodermis layer of specimens in Group B

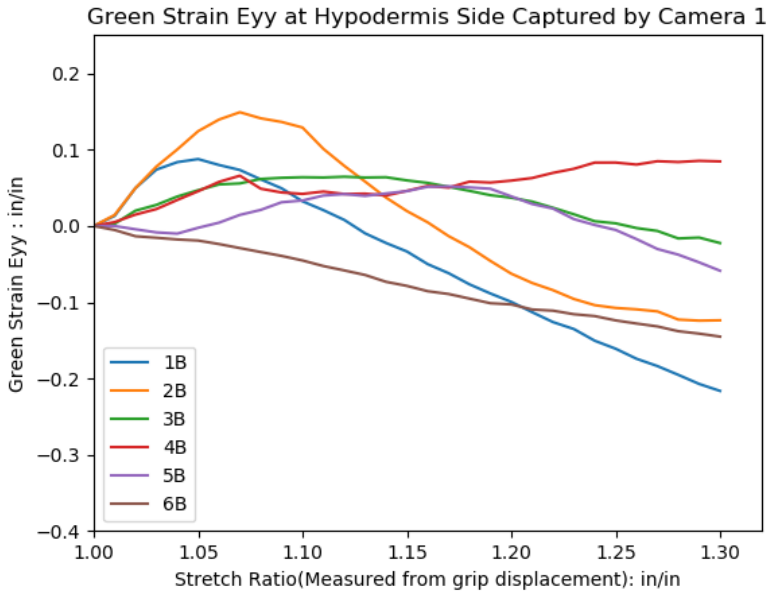

Figure 4.24: Exy of the hypodermis layer of specimens in Group B

Table 4.3: Strain for the epidermis and hypodermis layers of Group A at 30% Stretch

Sample	Exx(E)	Eyy(E)	Exy(E)	Exx(H)	Eyy(H)	Exy(H)
1A	0.30	-0.19	0.20	0.42	0.11	-0.55
2A	0.27	-0.27	0.03	0.16	-0.05	-0.03
3A	0.30	-0.31	-0.04	0.35	-0.19	0.08
4A	0.37	-0.22	-0.01	0.21	0.17	0.09
5A	0.28	-0.27	0.02	0.18	-0.22	-0.01
6A	0.34	-0.17	-0.21	0.54	-0.06	0.36
7A	0.40	-0.28	-0.08	0.35	-0.07	0.21
average	0.32	-0.25	-0.01	0.32	-0.05	0.02
std	0.05	0.05	0.12	0.14	0.14	0.29
max	0.40	-0.17	0.20	0.54	0.17	0.36
min	0.27	-0.31	-0.21	0.16	-0.22	-0.55

0.10, except 1A and 6A, which were 0.20 and -0.21 respectively.

The strain along the transverse direction, Eyy, decreased when the stretch increased (the magnitude of Eyy increased), as shown in Fig. 4.15. The average Eyy at 30% stretch was about -0.25, while the standard deviation was 0.05.

4.3.1.2 Specimens in Group B

Similarly, as the stretch increased, the Green strain along the stretching direction (Exx) at the epidermis layer increased(Fig. 4.19). The average Exx at 30% stretch was about 0.30, while the standard deviation was 0.04. Both of them were very close to those of specimens in Group A.

Shear strain Exy was less than 0.10, except 5B(0.24), as shown in Fig. 4.19.

Eyy decreased when the stretch increased (the magnitude of Eyy increased), as shown in Fig. 4.21. The average Eyy at 30% stretch was -0.25, while the standard deviation was 0.07. Note specimen 6B had a slight increase before decrease. We noticed that this specimen dangled more in the beginning compared to the rest of specimens in this group.

1A, 6A and 5B showed large shear (larger than 0.10). The authors suggested that this might be caused by the issue that there was an angle between the fiber orientation and the stretching axis.

Table 4.4: Strain for the epidermis and hypodermis layers of Group B at 30% Stretch

Sample	Exx(E)	Eyy(E)	Exy(E)	Exx(H)	Eyy(H)	Exy(H)
1B	0.27	-0.19	0.01	0.13	0.11	0.17
2B	0.35	-0.29	0.07	0.34	-0.22	0.03
3B	0.35	-0.34	0.04	0.32	-0.12	0.18
4B	0.30	-0.18	0.05	0.20	-0.02	-0.05
5B	0.29	-0.28	0.24	0.19	0.08	-0.26
6B	0.27	-0.21	0.05	0.24	-0.14	0.08
average	0.30	-0.25	0.08	0.24	-0.08	0.03
std	0.04	0.07	0.08	0.08	0.13	0.16
max	0.34	0.11	0.18	0.35	-0.18	0.24
min	0.13	-0.22	-0.26	0.27	-0.34	0.01

4.3.2 Hypodermis layer of specimens

4.3.2.1 Specimens in Group A

As the stretch increased, Exx at the hypodermis layer increased(Fig. 4.16). Compared to the epidermis layer of these specimens, the average Exx(0.32) at 30% stretch level was close to that of the epidermis layer of the same samples. The standard deviation(0.14) was more than twice as much as that. Note 1A, and 6A had much higher strains compared with the average, which were 0.42 and 0.54. In contrast, 2A, 4A and 5A had much lower strains compared with the average, which were 0.16, 0.21 and 0.18 respectively.

The magnitude of Exy of 1A, 6A and 7A were much larger than that of the rest of the specimens in this group, which were -0.55, 0.36 and 0.21 respectively, as shown in Fig. 4.17. The corresponding shear strains at the epidermis layers of these three specimens were 0.20(1A), -0.21(6A) and -0.08(7A). Note the trend of the shear strain between the hypodermis and the epidermis layers of these specimens were the same, but the hypodermis layers seemed to undergo more shear than the epidermis layers.

The Eyy of the specimens at the hypodermis layer seemed unpredictable(Fig. 4.18). As the stretch increased, some of them increased, some decreased, and the rest vibrated. Note 1A and

4A had positive Eyy at 30% stretch level, 0.11 and 0.17 respectively. 2A, 6A and 7A had negative Eyy (-0.05, -0.06, -0.07 respectively), but their magnitudes were much smaller compared with the epidermis layer (-0.27, -0.17 and -0.28 respectively).

Intuitively, under uniaxial loading, the specimen would contract at the transverse direction due to Poisson's effect. Thus the Eyy should be negative, and the magnitude should increase. However, the skin tissues had some curvatures after collection. The epidermis layer curved to hypodermis layer. Under the uniaxial stretching, the hypodermis layer tended to expand first before contracting. Additionally, 1A and 6A had tearing during the testing, which need to be taken into consideration when evaluating the strain.

4.3.2.2 Specimens in Group B

As the stretch increased, Exx at the hypodermis layer increased(Fig. 4.22). However, the average Exx(0.24) was smaller than that of the epidermis layer of the same samples, and the standard deviation(0.08) was larger. Note 2B had a sudden increase at around 22% stretch level. 1B, 4B, and 5B had much lower Exx at the hypodermis layer (0.13, 0.20 and 0.19 respectively) than the epidermis layer(0.27, 0.30 and 0.29 respectively).

Note 2B, 4B and 6B had shear strain Exy at 30% stretch less than 0.10, as shown in Fig. 4.23. 5B had a shear strain of -0.26, while its shear strain at the epidermis layer was 0.24, which indicated that the shear between these two surfaces were very close.

We noticed that 5B had slight tearing on the hypodermis layer at the clamping site. This might have some effects on strain measurement.

Note one interesting fact was that when a large shear happened in the hypodermis layer, there might not be shear at the epidermis layer, for example 7A. However, as long as the epidermis layer of a specimen encountered a shear larger than 0.10, there would always be a corresponding shear larger than 0.1 at the hypodermis layer, for example 1A, 6A, and 5B.

Similar to the Eyy at the hypodermis layer of specimens in Group A, the Eyy were unpredictable, as shown in Fig. 4.24. 1B and 5B had positive Eyy at 30% stretch. 3B, 4B and 6B had negative Eyy, but their magnitude were much smaller than that of the epidermis layer(-0.12, -0.02

and 0.08 respectively). This seems very similar as the hypodermis layer in Group A.

The difference between Exx of the epidermis layers of sub-samples in these two groups is not significant(p=0.5029). The difference between Eyy of the epidermis layers of sub-samples in these two groups is not significant(p=0.9197).

The difference between Exx of the hypodermis layers of sub-samples in these two groups is not significant(p=0.2557). The difference between Eyy of the hypodermis layers of sub-samples in these two groups is not significant(p=0.9378).

These indicate that the camera setup did not have too much effects on the strain measurement.

Thus we combined group 1 and 2 and analyzed the difference between strain of the epidermis and hypodermis layers of all the samples. The difference of Exx between the two layers is not significant(p=0.2398). The difference of Eyy between the epidermis and hypodermis layers of the samples is significant(p=0.000043)

4.4 Conclusions

This work shows that by measuring and comparing the strain of the hypodermis and epidermis layers of rat skin specimens, even when skin specimens are very thin, the strains are not always the same under the same loading condition. Thus it might be necessary to take into consideration the deformation of the hypodermis layer of soft tissues when trying to characterize their mechanical properties.

One of the possible reasons for this could be that the hypodermis layer (mostly composed of connective tissues) behaved differently from the epidermis layer due to the fact that they have different material constitutes. And the fiber orientation could also be different between these two layers.

We observed that the hypodermis layers of 1A teared slightly at the clamping site. 6A also had slight tearing in the hypodermis layer somewhere between the moving clamp and the beads. These might have effects on strain measurement. The occurence of tearing could be that some part of the hypodermis layer is slightly weaker or less extensive than the epidermis layer. It could also be that the technique we used in removing the loose connective tissue caused some damage to the

hypodermis layer. A more robust and reliable method is necessary to lathe off the loose connective tissues.

Note here we address that the trends were the same is because when the cameras were set at two sides of the specimen, the stretching axis is in the same direction as the +X axis of Camera 1, but opposite to the +X axis of Camera 2. Thus, if the two sides of a specimen were sheared the same angle, the measurement from one camera should be positive, while the other should be negative(Fig. 6).

In addition, it is challenging to completely remove the loosely connected soft tissue attached to the hypodermis layer. Thus it might interfere with the measurement of the deformation on the hypodermis layer.

The authors cut the specimens along across cranial-caudal direction directly. In the future study, it might be necessary to put these specimens under microscope to determine its fiber orientation before cutting. This might help explain how shear happened in the tests.

5. CONCLUSION

In this dissertation, a biaxial mechanical testing system has been designed with a particular emphasis on enabling the testing biologic tissues and tissue-engineered constructs. The design has been guided by new non-linear frameworks in theoretical mechanics that incorporate intuitive physically meaningful parameters. Moreover, a wide variety of clamping mechanisms and strain measurement techniques for soft tissues have been evaluated.

This work constitutes the first step in the development of a testing system and protocols that may potentially serve as the basis for the development of ASTM and ISO mechanical testing standards for biologic tissues. Such standards are presently critically limited. Future work will include the development of software applications designed to automate the mechanical testing process and subsequent acquisition of appropriate model parameters. Ultimately, the system and approach provide a broader set of physically meaningful parameters enabling a more comprehensive description of the complex mechanical behaviors observed in soft tissues. It is anticipated that this will significantly improve efforts to produce tissue-engineered constructs that are biomimetic with respect to mechanical behavior.

REFERENCES

[1] D. L. Butler, E. S. Grood, F. R. Noyes, R. F. Zernicke, and K. Brackett, "Effects of structure and strain measurement technique on the material properties of young human tendons and fascia," *Journal of Biomechanics*, vol. 17, no. 8, pp. 579–596, 1984.

[2] J. T.-M. Cheung and M. Zhang, "A serrated jaw clamp for tendon gripping," *Medical Engineering & Physics*, vol. 28, no. 4, pp. 379–382, 2006.

[3] D. Shi, D. Wang, C. Wang, and A. Liu, "A novel, inexpensive and easy to use tendon clamp for in vitro biomechanical testing," *Medical Engineering & Physics*, vol. 34, no. 4, pp. 516–520, 2012.

[4] D. Wright and D. Rennels, "A study of the elastic properties of plantar fascia," *JBJS*, vol. 46, no. 3, pp. 482–492, 1964.

[5] S.-Y. Woo, M. Ritter, D. Amiel, T. Sanders, M. Gomez, S. Kuei, S. Garfin, and W. Akeson, "The biomechanical and biochemical properties of swine tendons—long term effects of exercise on the digital extensors," *Connective Tissue Research*, vol. 7, no. 3, pp. 177–183, 1980.

[6] K. H. Svendsen and G. Thomson, "A new clamping and stretching procedure for determination of collagen fiber stiffness and strength relations upon maturation," *Journal of Biomechanics*, vol. 17, no. 3, pp. 225–229, 1984.

[7] D. Riemersa and H. Schamhardt, "The cryo-jaw, a clamp designed for in vitro rheology studies of horse digital flexor tendons," *Journal of Biomechanics*, vol. 15, no. 8, pp. 619–620, 1982.

[8] M.-O. Kiss, N. Hagemeister, A. Levasseur, J. Fernandes, B. Lussier, and Y. Petit, "A low-cost thermoelectrically cooled tissue clamp for in vitro cyclic loading and load-to-failure testing of muscles and tendons," *Medical Engineering & Physics*, vol. 31, no. 9, pp. 1182–1186, 2009.

[9] F. C. Yin, W. R. Tompkins, K. L. Peterson, and M. Intaglietta, "A video-dimension analyzer," *IEEE Transactions on Biomedical Engineering*, no. 5, pp. 376–381, 1972.

[10] J. Humphrey, D. Vawter, and R. Vito, "Quantification of strains in biaxially tested soft tissues," *Journal of Biomechanics*, vol. 20, no. 1, pp. 59–65, 1987.

[11] M. S. Sacks and W. Sun, "Multiaxial mechanical behavior of biological materials," *Annual Review of Biomedical Engineering*, vol. 5, no. 1, pp. 251–284, 2003.

[12] M. S. Sacks, "Biaxial mechanical evaluation of planar biological materials," *Journal of Elasticity and the Physical Science of Solids*, vol. 61, no. 1-3, p. 199, 2000.

[13] G. M. Cooney, K. M. Moerman, M. Takaza, D. C. Winter, and C. K. Simms, "Uniaxial and biaxial mechanical properties of porcine linea alba," *Journal of the Mechanical Behavior of Biomedical Materials*, vol. 41, pp. 68–82, 2015.

[14] V. Deplano, M. Boufi, O. Boiron, C. Guivier-Curien, Y. Alimi, and E. Bertrand, "Biaxial tensile tests of the porcine ascending aorta," *Journal of Biomechanics*, vol. 49, no. 10, pp. 2031–2037, 2016.

[15] B. Röhrnbauer, Y. Ozog, J. Egger, E. Werbrouck, J. Deprest, and E. Mazza, "Combined biaxial and uniaxial mechanical characterization of prosthetic meshes in a rabbit model," *Journal of Biomechanics*, vol. 46, no. 10, pp. 1626–1632, 2013.

[16] A. Avanzini, D. Battini, L. Bagozzi, and G. Bisleri, "Biomechanical evaluation of ascending aortic aneurysms," *BioMed Research International*, vol. 2014, 2014.

[17] S. J. Manoogian, J. A. Bisplinghoff, A. R. Kemper, and S. M. Duma, "Dynamic material properties of the pregnant human uterus," *Journal of Biomechanics*, vol. 45, no. 9, pp. 1724–1727, 2012.

[18] S. J. Manoogian, J. A. Bisplinghoff, C. McNally, A. R. Kemper, A. C. Santago, and S. M. Duma, "Dynamic tensile properties of human placenta," *Journal of Biomechanics*, vol. 41, no. 16, pp. 3436–3440, 2008.

[19] S. J. Manoogian, J. A. Bisplinghoff, C. McNally, A. R. Kemper, A. C. Santago, and S. M. Duma, "Effect of strain rate on the tensile material properties of human placenta," *Journal of Biomechanical Engineering*, vol. 131, no. 9, p. 091008, 2009.

[20] D.-L. Guo, B.-S. Chen, and N.-S. Liou, "Investigating full-field deformation of planar soft tissue under simple-shear tests," *Journal of Biomechanics*, vol. 40, no. 5, pp. 1165–1170, 2007.

[21] J. A. Weiss, J. C. Gardiner, and C. Bonifasi-Lista, "Ligament material behavior is nonlinear, viscoelastic and rate-independent under shear loading," *Journal of Biomechanics*, vol. 35, no. 7, pp. 943–950, 2002.

[22] J. C. Gardiner and J. A. Weiss, "Simple shear testing of parallel-fibered planar soft tissues," *Journal of Biomechanical Engineering*, vol. 123, no. 2, pp. 170–175, 2001.

[23] A. International, *ASTM D638-14, Standard Test Method for Tensile Properties of Plastics*. ASTM International, 2015.

[24] E. Mönch and D. Galster, "A method for producing a defined uniform biaxial tensile stress field," *British Journal of Applied Physics*, vol. 14, no. 11, p. 810, 1963.

[25] A. Avanzini and D. Battini, "Integrated experimental and numerical comparison of different approaches for planar biaxial testing of a hyperelastic material," *Advances in Materials Science and Engineering*, vol. 2016, 2016.

[26] N. T. Jacobs, D. H. Cortes, E. J. Vresilovic, and D. M. Elliott, "Biaxial tension of fibrous tissue: using finite element methods to address experimental challenges arising from boundary conditions and anisotropy," *Journal of Biomechanical Engineering*, vol. 135, no. 2, p. 021004, 2013.

[27] S. Waldman, M. Sacks, and J. Lee, "Boundary conditions during biaxial testing of planar connective tissues part ii fiber orientation," *Journal of Materials Science Letters*, vol. 21, no. 15, pp. 1215–1221, 2002.

[28] S. D. Waldman and J. M. Lee, "Boundary conditions during biaxial testing of planar connective tissues. part 1: dynamic behavior," *Journal of Materials Science: Materials in Medicine*, vol. 13, no. 10, pp. 933–938, 2002.

[29] W. Sun, M. S. Sacks, and M. J. Scott, "Effects of boundary conditions on the estimation of the planar biaxial mechanical properties of soft tissues," *Journal of Biomechanical Engineering*, vol. 127, no. 4, pp. 709–715, 2005.

[30] R. Simón-Allué, A. Cordero, and E. Peña, "Unraveling the effect of boundary conditions and strain monitoring on estimation of the constitutive parameters of elastic membranes by biaxial tests," *Mechanics Research Communications*, vol. 57, pp. 82–89, 2014.

[31] P. Nielsen, P. Hunter, and B. Smaill, "Biaxial testing of membrane biomaterials: testing equipment and procedures," *Journal of Biomechanical Engineering*, vol. 113, no. 3, pp. 295–300, 1991.

[32] F. C. Yin, P. H. Chew, and S. L. Zeger, "An approach to quantification of biaxial tissue stress-strain data," *Journal of Biomechanics*, vol. 19, no. 1, pp. 27–37, 1986.

[33] M. S. Sacks and C. Chuong, "Orthotropic mechanical properties of chemically treated bovine pericardium," *Annals of Biomedical Engineering*, vol. 26, no. 5, pp. 892–902, 1998.

[34] S. Dokos, B. H. Smaill, A. A. Young, and I. J. LeGrice, "Shear properties of passive ventricular myocardium," *American Journal of Physiology-Heart and Circulatory Physiology*, vol. 283, no. 6, pp. H2650–H2659, 2002.

[35] S. Dokos, I. J. LeGrice, B. H. Smaill, J. Kar, and A. A. Young, "A triaxial-measurement shear-test device for soft biological tissues," *Journal of Biomechanical Engineering*, vol. 122, no. 5, pp. 471–478, 2000.

[36] Y. Lanir and Y. Fung, "Two-dimensional mechanical properties of rabbit skin—i. experimental system," *Journal of Biomechanics*, vol. 7, no. 1, pp. 29–34, 1974.

[37] K. L. Billiar and M. S. Sacks, "Biaxial mechanical properties of the natural and glutaraldehyde treated aortic valve cusp—part i: experimental results," *Journal of Biomechanical Engineering*, vol. 122, no. 1, pp. 23–30, 2000.

[38] J. S. Grashow, A. P. Yoganathan, and M. S. Sacks, "Biaixal stress–stretch behavior of the mitral valve anterior leaflet at physiologic strain rates," *Annals of Biomedical Engineering*, vol. 34, no. 2, pp. 315–325, 2006.

[39] P. G. Charette, I. W. Hunter, and P. J. Hunter, "Large deformation mechanical testing of biological membranes using speckle interferometry in transmission. i: Experimental apparatus," *Applied Optics*, vol. 36, no. 10, pp. 2238–2245, 1997.

[40] P. G. Charette, P. J. Hunter, and I. W. Hunter, "Large deformation mechanical testing of biological membranes using speckle interferometry in transmission. ii: Finite element modeling," *Applied Optics*, vol. 36, no. 10, pp. 2246–2251, 1997.

[41] S. A. Yavari, J. van der Stok, H. Weinans, and A. A. Zadpoor, "Full-field strain measurement and fracture analysis of rat femora in compression test," *Journal of Biomechanics*, vol. 46, no. 7, pp. 1282–1292, 2013.

[42] K. Genovese, Y. Lee, and J. Humphrey, "Novel optical system for in vitro quantification of full surface strain fields in small arteries: I. theory and design," *Computer Methods in Biomechanics and Biomedical Engineering*, vol. 14, no. 03, pp. 213–225, 2011.

[43] D. S. Zhang and D. D. Arola, "Applications of digital image correlation to biological tissues," *Journal of Biomedical Optics*, vol. 9, no. 4, pp. 691–700, 2004.

[44] S. D. Waldman and J. M. Lee, "Boundary conditions during biaxial testing of planar connective tissues. part 1: dynamic behavior," *Journal of Materials Science: Materials in Medicine*, vol. 13, no. 10, pp. 933–938, 2002.

[45] L. Scalise, B. Lonzi, and N. Bernacchia, "A camera-based experimental method for mechanical test on patellar tendons," in *Mechanics of Biological Systems and Materials, Volume 7*, pp. 7–17, Springer, 2015.

[46] A. Probst, D. Palmes, H. Freise, M. Langer, A. Joist, and H. Spiegel, "A new clamping technique for biomechanical testing of tendons in small animals," *Journal of Investigative Surgery*, vol. 13, no. 6, pp. 313–318, 2000.

[47] P. Wieloch, G. Buchmann, W. Roth, and M. Rickert, "A cryo-jaw designed for in vitro tensile testing of the healing achilles tendons in rats," *Journal of Biomechanics*, vol. 37, no. 11, pp. 1719–1722, 2004.

[48] M. Abrahamson, "Mechanical behaviour of tendon in vitro: a preliminary report," *Medical and Biological Engineering*, vol. 5, pp. 433–443, 1967.

[49] J. C. Iatridis, J. Wu, J. A. Yandow, and H. M. Langevin, "Subcutaneous tissue mechanical behavior is linear and viscoelastic under uniaxial tension," *Connective Tissue Research*, vol. 44, no. 5, pp. 208–217, 2003.

[50] M. Lyons, D. C. Winter, and C. K. Simms, "Mechanical characterisation of porcine rectus sheath under uniaxial and biaxial tension," *Journal of Biomechanics*, vol. 47, no. 8, pp. 1876–1884, 2014.

[51] A. Viidik, "Experimental evaluation of the tensile strength of isolated rabbit tendons," *Biomedical Engineering*, no. 2, pp. 64–67, 1967.

[52] P. Soden and I. Kershaw, "Tensile testing of connective tissues," *Medical and Biological Engineering*, vol. 12, no. 4, pp. 510–518, 1974.

[53] M. Bennett, R. Ker, N. J. Imery, and R. M. Alexander, "Mechanical properties of various mammalian tendons," *Journal of Zoology*, vol. 209, no. 4, pp. 537–548, 1986.

[54] R. Cohen, C. Hooley, and N. McCrum, "Viscoelastic creep of collagenous tissue," *Journal of Biomechanics*, vol. 9, no. 4, pp. 175–184, 1976.

[55] R. F. Ker, "Mechanics of tendon, from an engineering perspective," *International Journal of Fatigue*, vol. 29, no. 6, pp. 1001–1009, 2007.

[56] X. T. Wang and R. F. Ker, "Creep rupture of wallaby tail tendons.," *Journal of Experimental Biology*, vol. 198, no. 3, pp. 831–845, 1995.

[57] N. Ramachandran, Y. Koike, P. Poitras, D. Backman, H. K. Uhthoff, and G. Trudel, "Dual cryogenic fixation for mechanical testing of soft musculoskeletal tissues," *IEEE Transactions on Biomedical Engineering*, vol. 52, no. 10, pp. 1792–1795, 2005.

[58] J. Lepetit, R. Favier, A. Grajales, and P. Skjervold, "A simple cryogenic holder for tensile testing of soft biological tissues," *Journal of Biomechanics*, vol. 37, no. 4, pp. 557–562, 2004.

[59] N. A. Sharkey, T. S. Smith, and D. C. Lundmark, "Freeze clamping musculo-tendinous junctions for in vitro simulation of joint mechanics," *Journal of Biomechanics*, vol. 28, no. 5, pp. 631–635, 1995.

[60] R. Ker, N. J. Dimery, and R. M. Alexander, "The role of tendon elasticity in hopping in a wallaby (macropus rufogriseus)," *Journal of Zoology*, vol. 208, no. 3, pp. 417–428, 1986.

[61] P. L. Blanton and N. L. Biggs, "Ultimate tensile strength of fetal and adult human tendons," *Journal of Biomechanics*, vol. 3, no. 2, pp. 181–184, 1970.

[62] R. F. Ker, "Dynamic tensile properties of the plantaris tendon of sheep (ovis aries)," *Journal of Experimental Biology*, vol. 93, no. 1, pp. 283–302, 1981.

[63] A. R. Kemper, A. C. Santago, J. D. Stitzel, J. L. Sparks, and S. M. Duma, "Biomechanical response of human liver in tensile loading," in *Annals of Advances in Automotive Medicine/Annual Scientific Conference*, vol. 54, p. 15, Association for the Advancement of Automotive Medicine, 2010.

[64] V. Roth and V. Mow, "The intrinsic tensile behavior of the matrix of bovine articular cartilage and its variation with age.," *The Journal of Bone and Joint Surgery. American volume*, vol. 62, no. 7, pp. 1102–1117, 1980.

[65] J. Mansour, B. Davis, M. Srour, and R. Theberge, "A method for obtaining repeatable measurements of the tensile properties of skin at low strain," *Journal of Biomechanics*, vol. 26, no. 2, pp. 211–216, 1993.

[66] K. Komatsu, C. Sanctuary, T. Shibata, A. Shimada, and J. Botsis, "Stress–relaxation and microscopic dynamics of rabbit periodontal ligament," *Journal of Biomechanics*, vol. 40, no. 3, pp. 634–644, 2007.

[67] C. S. Enwemeka, "The effects of therapeutic ultrasound on tendon healing. a biomechanical study.," *American Journal of Physical Medicine & Rehabilitation*, vol. 68, no. 6, pp. 283–287, 1989.

[68] T. Nilsson, "Biomechanical studies of rabbit abdominal wall. part i.—the mechanical properties of specimens from different anatomical positions," *Journal of Biomechanics*, vol. 15, no. 2, pp. 123–129, 1982.

[69] D. Stromberg and C. Wiederhielm, "Viscoelastic description of a collagenous tissue in simple elongation," *Journal of Applied Physiology*, vol. 26, no. 6, pp. 857–862, 1969.

[70] T. M. Best, A. Collins, E. G. Lilly, A. V. Seaber, R. Goldner, and G. A. Murrell, "Achilles tendon healing: a correlation between functional and mechanical performance in the rat," *Journal of Orthopaedic Research*, vol. 11, no. 6, pp. 897–906, 1993.

[71] G. A. Murrell, E. G. Lilly III, R. D. Goldner, A. V. Seaber, and T. M. Best, "Effects of immobilization on achilles tendon healing in a rat model," *Journal of Orthopaedic Research*, vol. 12, no. 4, pp. 582–591, 1994.

[72] P. P. Purslow, T. J. Wess, and D. Hukins, "Collagen orientation and molecular spacing during creep and stress-relaxation in soft connective tissues.," *Journal of Experimental Biology*, vol. 201, no. 1, pp. 135–142, 1998.

[73] D. Elliott, "The biomechanical properties of tendon in relation to muscular strength," *Rheumatology*, vol. 9, no. 1, pp. 1–7, 1967.

[74] J. V. Benedict, L. B. Walker, and E. H. Harris, "Stress-strain characteristics and tensile strength of unembalmed human tendon," *Journal of Biomechanics*, vol. 1, no. 1, p. IN11, 1968.

[75] R. Welsh, I. Macnab, and V. Riley, "Biomechanical studies of rabbit tendon," *Clinical Orthopaedics and Related Research®*, vol. 81, pp. 171–177, 1971.

[76] L. B. Walker, E. H. Harris, and J. V. Benedict, "Stress-strain relationship in human cadaveric plantaris tendon: a preliminary study," *Medical Electronics and Biological Engineering*, vol. 2, no. 1, pp. 31–38, 1964.

[77] S.-Y. Woo, M. Gomez, D. Amiel, M. Ritter, R. Gelberman, and W. Akeson, "The effects of exercise on the biomechanical and biochemical properties of swine digital flexor tendons," *Journal of Biomechanical Engineering*, vol. 103, no. 1, pp. 51–56, 1981.

[78] R. Haut, "Age-dependent influence of strain rate on the tensile failure of rat-tail tendon," *Journal of Biomechanical Engineering*, vol. 105, no. 3, pp. 296–299, 1983.

[79] C. Smith, I. Young, and J. Kearney, "Mechanical properties of tendons: changes with sterilization and preservation," *Journal of Biomechanical Engineering*, vol. 118, no. 1, pp. 56–61, 1996.

[80] X. T. Wang, R. F. Ker, and R. M. Alexander, "Fatigue rupture of wallaby tail tendons.," *Journal of Experimental Biology*, vol. 198, no. 3, pp. 847–852, 1995.

[81] R. F. Ker, X. T. Wang, and A. Pike, "Fatigue quality of mammalian tendons," *Journal of Experimental Biology*, vol. 203, no. 8, pp. 1317–1327, 2000.

[82] K. Vilendrer, K. Grimes, J. Shukla, D. Strei, C. Eriksen, and T. Nickel, "Thermo-electric grip for holding soft tissue," Apr. 15 2003. US Patent 6,547,783.

[83] K. D. Klinich, C. S. Miller, J. Hu, G. M. Nazmi, M. D. Pearlman, L. W. Schneider, and J. D. Rupp, "Effect of frozen storage on dynamic tensile properties of human placenta," *Journal of Biomechanical Engineering*, vol. 134, no. 3, p. 034501, 2012.

[84] P. Schöttle, I. Goudakos, N. Rosenstiel, J.-E. Hoffmann, W. R. Taylor, G. N. Duda, and M. O. Heller, "A comparison of techniques for fixation of the quadriceps muscle–tendon complex for in vitro biomechanical testing of the knee joint in sheep," *Medical Engineering & Physics*, vol. 31, no. 1, pp. 69–75, 2009.

[85] Y. Lanir and Y. Fung, "Two-dimensional mechanical properties of rabbit skin—i. experimental system," *Journal of Biomechanics*, vol. 7, no. 1, pp. 29–34, 1974.

[86] Y. Lanir and Y. Fung, "Two-dimensional mechanical properties of rabbit skin—ii. experimental results," *Journal of Biomechanics*, vol. 7, no. 2, pp. 171–182, 1974.

[87] J. M. Lee and D. R. Boughner, "Tissue mechanics of canine pericardium in different test environments. evidence for time-dependent accommodation, absence of plasticity, and new roles for collagen and elastin.," *Circulation Research*, vol. 49, no. 2, pp. 533–544, 1981.

[88] J. M. Lee, D. W. Courtman, and D. R. Boughner, "The glutaraldehyde-stabilized porcine aortic valve xenograft. i. tensile viscoelastic properties of the fresh leaflet material," *Journal of Biomedical Materials Research*, vol. 18, no. 1, pp. 61–77, 1984.

[89] J. M. Lee, D. W. Courtman, and D. R. Boughner, "The glutaraldehyde-stabilized porcine aortic valve xenograft. i. tensile viscoelastic properties of the fresh leaflet material," *Journal of Biomedical Materials Research*, vol. 18, no. 1, pp. 61–77, 1984.

[90] C. S. Shah, M. J. Mason, K. H. Yang, W. N. Hardy, C. A. Van Ee, R. Morgan, and K. Digges, "High-speed biaxial tissue properties of the human cadaver aorta," in *ASME 2005 International Mechanical Engineering Congress and Exposition*, pp. 103–111, American Society of Mechanical Engineers, 2005.

[91] C. Oehman, M. Baleani, and M. Viceconti, "Repeatability of experimental procedures to determine mechanical behaviour of ligaments," *Acta Bioeng Biomech*, vol. 11, pp. 19–23, 2009.

[92] J. Downs, H. R. Halperin, J. Humphrey, and F. Yin, "An improved video-based computer tracking systems for soft biomaterials testing," *IEEE Transactions on Biomedical Engineering*, vol. 37, no. 9, pp. 903–907, 1990.

[93] X. Shang, M. R. Yen, and M. W. Gaber, "Studies of biaxial mechanical properties and nonlinear finite element modeling of skin," *Molecular & Cellular Biomechanics*, vol. 7, no. 2, pp. 93–104, 2010.

[94] M. Griffin, Y. Premakumar, A. Seifalian, P. E. Butler, and M. Szarko, "Biomechanical characterization of human soft tissues using indentation and tensile testing," *Journal of Visualized Experiments: JoVE*, no. 118, 2016.

[95] Y. Kvistedal and P. Nielsen, "Estimating material parameters of human skin in vivo," *Biomechanics and Modeling in Mechanobiology*, vol. 8, no. 1, pp. 1–8, 2009.

[96] A. N. Annaidh, K. Bruyère, M. Destrade, M. D. Gilchrist, and M. Otténio, "Characterization of the anisotropic mechanical properties of excised human skin," *Journal of the Mechanical Behavior of Biomedical Materials*, vol. 5, no. 1, pp. 139–148, 2012.

[97] E. Rizzuto, S. Carosio, and Z. Del Prete, "Characterization of a digital image correlation system for dynamic strain measurements of small biological tissues," *Experimental Techniques*, vol. 40, no. 2, pp. 743–753, 2016.

[98] A. H. Hoffman and P. Grigg, "A method for measuring strains in soft tissue," *Journal of Biomechanics*, vol. 17, no. 10, pp. 795–800, 1984.

APPENDIX A

BIAXIAL SYSTEM USER MANUAL

A.1 Operation Procedure

1. Press the button on the main power outlet

2. Turn on the power of the controller and instrumentation chassis respectively.

3. Open the "Kollmorgen Workbench" software(Fig. A.1)

4. Select a drive(Fig. A.2)

5. Connect a drive(Fig.A.3)

6. Open the BIAX.exe software (Fig. A.4)

7. Ping the controller and then connect to controller(Fig. A.5)

8. Then turn on the controller(Fig. A.6)

9. Open the "Setpoint"(Fig. A.7)

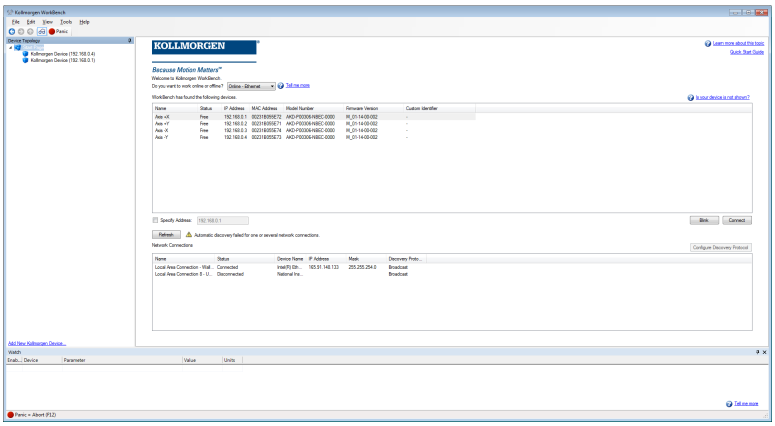

Figure A.1: Open Kollmorgen software

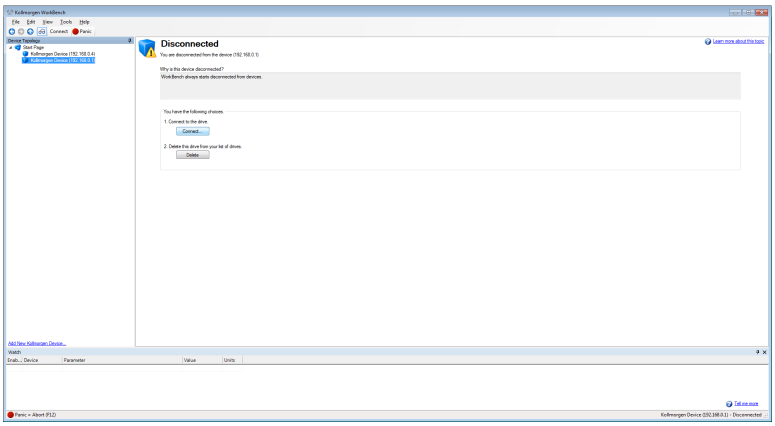

Figure A.2: Select a drive

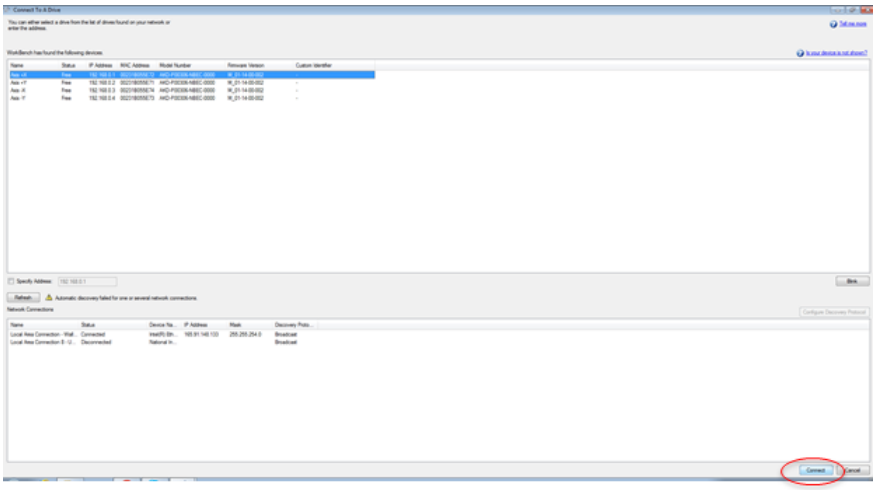

Figure A.3: Connect a drive

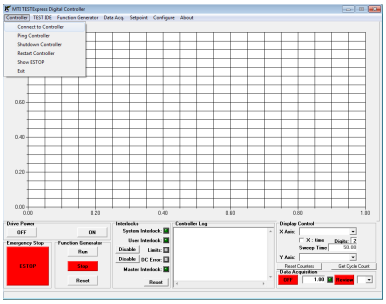

Figure A.4: Controller module of BIAX software

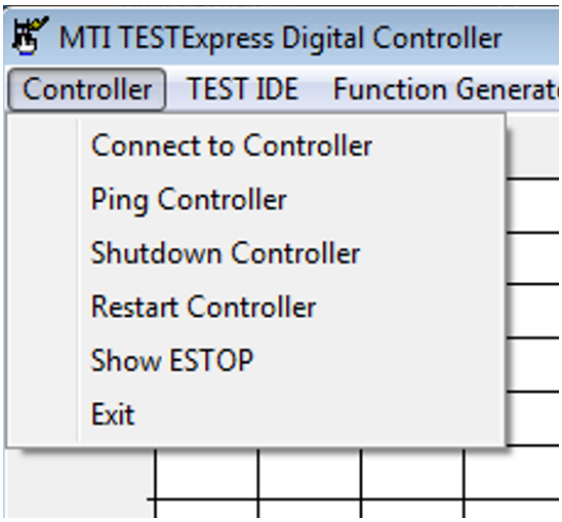

Figure A.5: Ping the controller

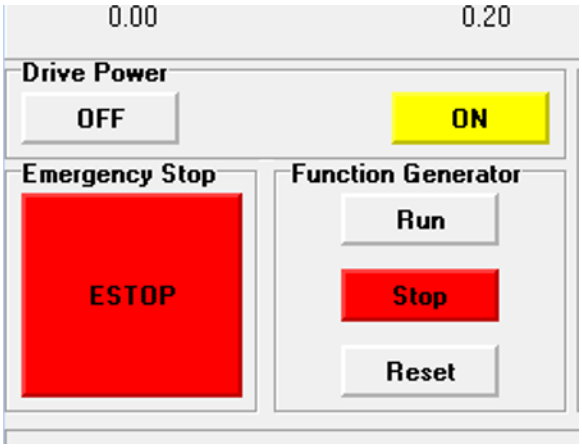

Figure A.6: Turn on a controller

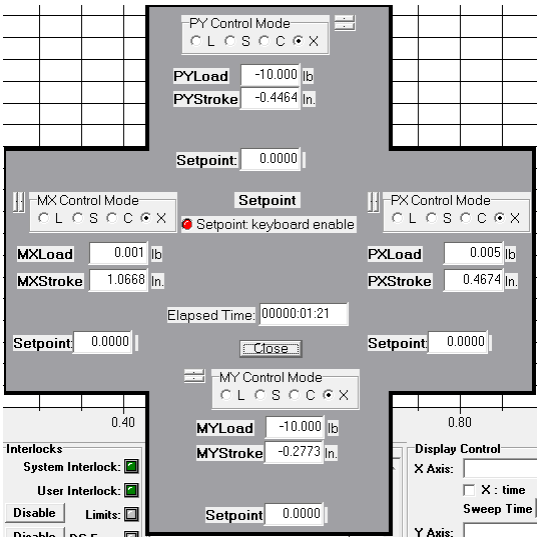

Figure A.7: Open the setpoint

10. Press "Ctrl" and select a control mode, S for "displacement", L for "load" and C for "centroid" control

11. Open the "Function Generators"(Fig. A.8), there are in total four types function generators (Fig. A.9).

12. Click on the "Axis" first, then Select an option for "End Point" and input a value for "Rate" or "Time"

13. Select a function generator for this "Axis", then close the "Function Generators" dialog

14. Click "Data Acq" and select "Synch to F.G." to synchronize the data acquisition to the function generator (Fig. A.10)

15. Click "report Defaults" and select "Voltage" to obtain the raw data output (Fig. A.11)

16. Go to the controller interface, click "Run" to start the function generator. Stop the motion by clicking "Stop" (Fig. A.12)

17. When exit the program, click the "Off" first(Fig. A.13), the click "Exit" in the control block (Fig. A.5)

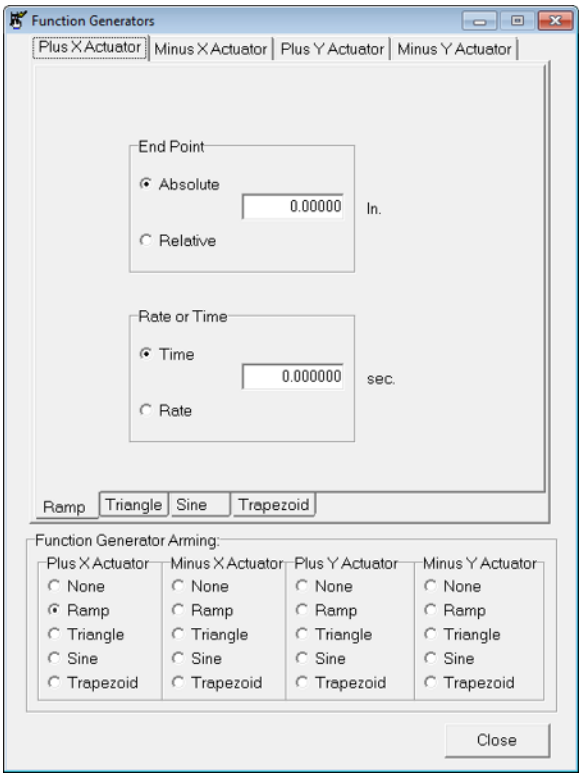

Figure A.8: Function generator

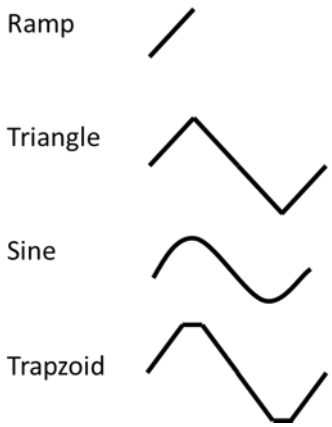

Figure A.9: Function generator types

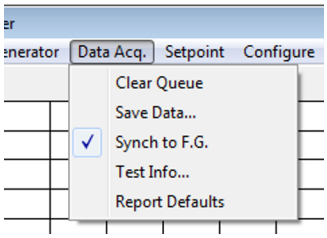

Figure A.10: Data acquisition

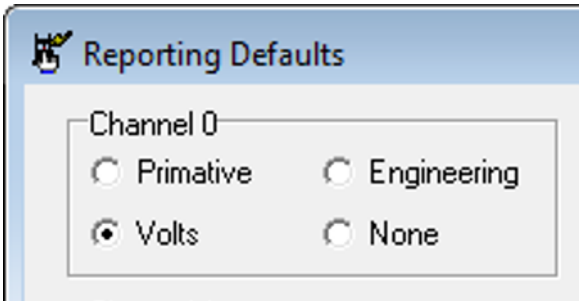

Figure A.11: Report default

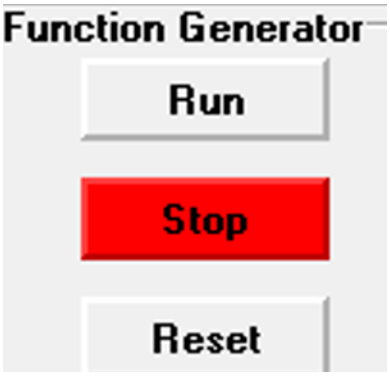

Figure A.12: Function generator control

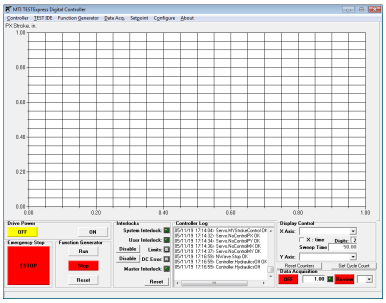

Figure A.13: Turn off the controller

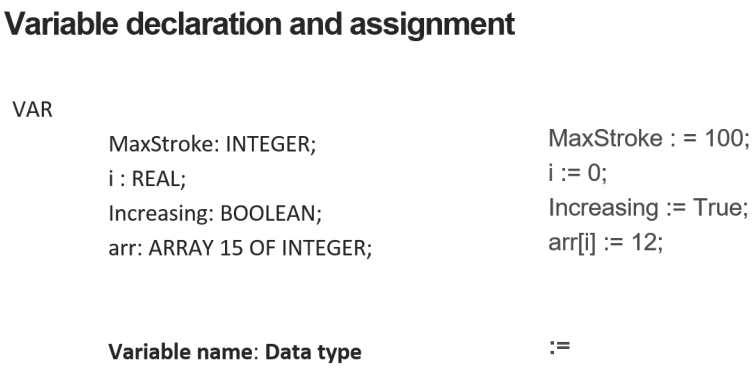

Figure A.14: Variable declaration and assignment

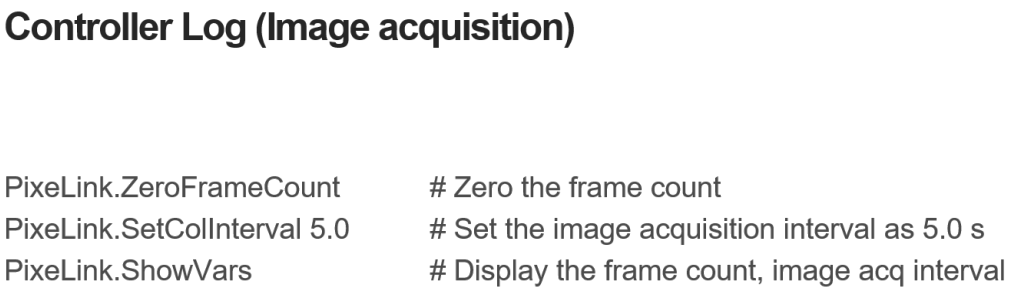

Figure A.15: Image acquisition commands

A.2 Script

The instructions for the programming language used in this controller are listed below:

Input/Output

- In.Int(i) #Scan the integer parameter
- In.Real(x) #Scan the real parameter

- Out.Int(i, 5) #print the parameter
- Out.Real(r, 15)
- Out.Ln
- Out.String("hi");

Figure A.16: Input/output

Arithmetic expressions

- ENTIER(x) convert to long integer
- SHORT(i) short the long integer/integer
- INC(i) increase integer by one
- DEC(i) decrease integer by one
- DIV Integer division
- MOD modulus

Figure A.17: Arithmetic expression

Relations

- = Equal
- # Not equal
- <= less or equal
- >= greater or equal

Figure A.18: Relation

Statement(If)

MTI

```
IF Expression THEN
        StatementSequence;
ELSIF Expression THEN
        StatementSequence;
ELSE
        StatementSequence;
END;
```

Example

```
IF a > b THEN
        Out.String(“Hello”);
ELSIF a = b THEN
        Out.String(“Howdy”);
ELSE
        Out.String(“Hi”);
END;
```

Figure A.19: If statement

Statement(While)

MTI

```
WHILE Expression DO
        StatementSequence
END;
```

Example

```
WHILE i > 0 DO
        k := k +1;
END;
```

Figure A.20: While statement

Statement(Case)

MTI

```
CASE Expression OF
        Case: StatementSequence
        | Case: StatementSequence
ELSE
        StatementSequence
END;
```

Example

```
CASE Channel OF
        0: Out.String(“Hello”);
        |1: Out.String(“Howdy”);
ELSE
        Out.String(“Hi”);
END;
```

Figure A.21: Case statement

Statement(For)

MTI	FOR ident ":=" Expression TO Expression DO StatementSequence
Example	FOR i:= 0 TO 10 DO k := k + 1 END

Figure A.22: For statement

Ramp

```
Ramp = RECORD
      (*data elements:  Among others...: *)
      SLOPE        : LONGREAL; (* D/A units per tick *)
      ENDPT        : INTEGER;  (* D/A units *)
      RorT         : BOOLEAN;  (* Rate = TRUE; Time = FALSE *)
      REL          : BOOLEAN;  (* TRUE = relative end point *)
      LENGTH       : LONGINT;
      ITERATIONS    : LONGINT;
      WaveRunning,            (* state of wave *)
      NewWave:      : BOOLEAN;  (* instantiation flag *)

      (*methods:*)
      PROCEDURE OnFinalRamp(myObject: NWave.RampWaveDesc);

     END;
```

Figure A.23: Ramp funtion example

```
PROCEDURE SecondEndLevel(VAR myObject: NWave.RampWaveDesc);
 BEGIN

    myObject.ENDPT :=  - SHORT( ENTIER(EndPt) );  (* user supplied in test protocol *)
    myObject.LENGTH :=  ENTIER(Time * 1000);  (* user supplied in test protocol, Note
      the defult time value is in ms *)

    myObject.RorT  := FALSE;  (* always do this by RATE *)
    myObject.REL   := TRUE;  (* always do this on an absolute basis *)

    NWave.CommsFG[Channel].Rmp.ENDPT := myObject.ENDPT;
    NWave.CommsFG[Channel].Rmp.RorT := myObject.RorT;
    NWave.CommsFG[Channel].Rmp.REL  := myObject.REL;
    NWave.CommsFG[Channel].Rmp.LENGTH := myObject.LENGTH / 1000; (* convert back *)

    ControlData.SendFG := TRUE;
    myObject.NewWave := TRUE;
    myObject.WaveRunning := TRUE;  (* prevents FGRun mechanism from halting generator *)
    NWave.InstallOnFinalRamp(Channel, FirstEndLevel);
 END SecondEndLevel;
```

Figure A.24: Procedure example